

**SUBSTITUTION EFFECTS IN CrAs
SUPERCONDUCTOR**

BY

Mohammed Abdallah Khalid Abubaker

A Thesis Presented to the
DEANSHIP OF GRADUATE STUDIES

KING FAHD UNIVERSITY OF PETROLEUM & MINERALS

DHAHRAN, SAUDI ARABIA

In Partial Fulfillment of the
Requirements for the Degree of

MASTER OF SCIENCE

In

PHYSICS

DECEMBER, 2015

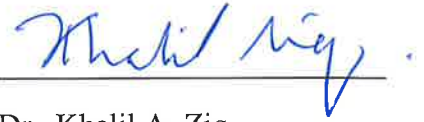
KING FAHD UNIVERSITY OF PETROLEUM & MINERALS

DHAHRAN- 31261, SAUDI ARABIA

DEANSHIP OF GRADUATE STUDIES

This thesis, written by **Mohammed Abdallah Khalid Abubaker** under the direction his thesis advisor and approved by his thesis committee, has been presented and accepted by the Dean of Graduate Studies, in partial fulfillment of the requirements for the degree of

MASTER OF SCIENCE IN PHYSICS.



Dr. Khalil A. Ziq
(Advisor)



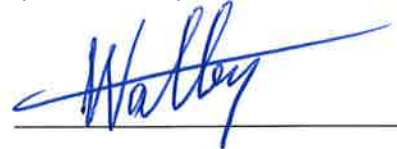
Dr. Abdullah A. Al-Sunaidi
Department Chairman



Dr. Mohamed Faiz
(Co-Advisor)



Dr. Salam A. Zummo
Dean of Graduate Studies



Dr. Watheq Al-Basheer
(Member)

5/4/16

Date



Dr. Abdelkrim Mekki
(Member)



Dr. Muhammad Haider
(Member)

© Mohammed Abdallah Khalid Abubaker

2015

Profound gratitude goes to Allah, for the invaluable gifts of life and wherewithal to complete the MS program.

ACKNOWLEDGMENTS

All praise and glory to ALLAH for giving me the good health, courage and patience to complete this work. Foremost, I would to express my heartfelt love and gratitude to my parents and family in Palestine for their support and help in overcoming the challenges I have faced during my study. Moreover, I would like to express my sincere gratitude to my adviser Prof. Khalil A. Ziq for the continuous support during the course of my graduate study and MS research program. I gracefully appreciate his patience, motivation, enthusiasm and immense knowledge. His guidance helped me see-through the dark alleys of research and writing of this thesis. I could not have imagined having a better adviser and mentor for my MS study in physics. Not the least, I am indebted to my thesis co-advisor, Dr. Mohamed Faiz for his teaching, guidance, empathy and completing the part that related to XPS in my thesis work. I would like to thank my thesis committee: Dr. Watheq Al-Basheer, Dr. Abdelkrium Mekki and Dr. Muhammad Haider for their encouragement and insightful comments. Special thank for Dr. Ahmad Salem for his motivation and support in using LABVIEW software. Last but not least, I would to thank KFUPM and physics Department for giving me this chance.

TABLE OF CONTENTS

ACKNOWLEDGMENTS	V
TABLE OF CONTENTS.....	VI
LIST OF TABLES	VIII
LIST OF FIGURES	IX
ABSTRACT.....	XII
ملخص الرسالة.....	XIII
CHAPTER 1 INTRODUCTION	1
1.1 Discovery of superconductivity	1
1.2 Basic properties of superconductor	1
1.3 Literature review	2
1.4 Thesis objective.....	9
CHAPTER 2 EXPERIMENTAL METHOD	10
2.1 Preparation of CrAs _{1-x} Sb _x samples	10
2.2 Characterization of the prepared samples	12
2.2.1 Transport measurement using closed cycle refrigerator	12
2.2.2 X-ray diffraction analysis	14
2.2.3 X-ray photoelectron spectroscopy (XPS) measurement	14
CHAPTER 3 X-RAY DIFFERATION ANALYSIS	16
3.1 Result and discussion	16
CHAPTER 4 X-RAY PHOTOELECTRON SPECTROSCOPY (XPS)	26
4.1 Introduction.....	26
4.2 Result and discussion	27

CHAPTER 5	TRANSPORT MEASUREMENTS.....	39
5.1	Introduction.....	39
5.2	Result and discussion.....	40
CHAPTER 6	CONCLUSION AND RECOMENDATION.....	50
6.1	Conclusion	50
6.2	Recommendation for future work.....	51
REFERENCES	52
VITAE.....	57

LIST OF TABLES

Table 2.1: Concentration of each constituent of $\text{CrAs}_{1-x}\text{Sb}_x$	11
Table 3.1: Structural parameters of $\text{CrAs}_{1-x}\text{Sb}_x$ samples	24
Table 4.1: Summary of the XPS analysis for $\text{CrAs}_{1-x}\text{Sb}_x$ samples	38
Table 5.1: Antiferromagnetic transition temperature T_N with concentration of Antimony for ($\text{CrAs}_{1-x}\text{Sb}_x$) samples and with applied pressure on CrAs as in [1].....	48

LIST OF FIGURES

Figure 1.1: Family of iron based superconductor[8].	4
Figure 1.2: phase diagram of $\text{CrAs}_{1-x}\text{Sb}_x$ [21].	6
Figure 1.3: Phase diagram of CrAs [1].	7
Figure 2.1: Platform step of the furnace for 12 samples of $\text{CrAs}_{1-x}\text{Sb}_x$	12
Figure 2.2: Schematic diagram of transport measurement (A.c set up).....	13
Figure 2.3: Schematic diagram of UHV chamber with other XPS components	15
Figure 3.1: X-ray diffraction pattern of CrAs with the phases of the peaks	16
Figure 3.2: X-ray diffraction pattern of $\text{CrAs}_{0.99}\text{Sb}_{0.01}$ with the phases of the peaks.....	17
Figure 3.3: X-ray diffraction pattern of $\text{CrAs}_{0.95}\text{Sb}_{0.05}$ with the phases of the peaks.....	17
Figure 3.4: X-ray diffraction pattern of $\text{CrAs}_{0.90}\text{Sb}_{0.10}$ with the phases of the peaks	18
Figure 3.5: X-ray diffraction pattern of $\text{CrAs}_{0.85}\text{Sb}_{0.15}$ with the phases of the peaks.....	18
Figure 3.6: X-ray diffraction pattern of $\text{CrAs}_{0.55}\text{Sb}_{0.45}$ with the phases of the peaks.....	19
Figure 3.7: X-ray diffraction pattern of $\text{CrAs}_{0.50}\text{Sb}_{0.50}$ with the phases of the peaks.....	19
Figure 3.8: X-ray diffraction pattern of $\text{CrAs}_{0.45}\text{Sb}_{0.55}$ with the phases of the peaks.....	20
Figure 3.9: X-ray diffraction pattern of $\text{CrAs}_{0.40}\text{Sb}_{0.60}$ with the phases of the peaks.....	20
Figure 3.10: X-ray diffraction pattern of $\text{CrAs}_{0.35}\text{Sb}_{0.65}$ with the phases of the peaks.....	21
Figure3.11: X-ray diffraction pattern of CrSb with the phases of the peaks	21
Figure 3.12: Variation of lattice parameters with the concentration of Sb in CrAs_{1-x} - Sb_x	25
Figure 3.13: Variation of the volume of unit cell with the concentration of Sb in $\text{CrAs}_{1-x}\text{Sb}_x$	25
Figure 4.1: Schematic diagram of the basic principle used in XPS.....	27

Figure 4.2: XPS spectra of CrAs sample: (a) Cr2p core level spectrum, (b) As3d core level spectrum. The experimental spectra are represented by solid line. The fitted peaks are represented by open triangle.	29
Figure 4.3: XPS spectra of CrAs _{0.55} Sb _{0.45} sample: (a) Cr2p core level spectrum, (b) As3d core level spectrum, (c) Sb3d core level spectrum. The experimental spectra are represented by solid line. The fitted peaks are represented by open triangle.....	31
Figure 4.4: XPS spectra of CrAs _{0.50} Sb _{0.50} sample: (a) Cr2p core level spectrum, (b) As3d core level spectrum, (c) Sb3d core level spectrum. The experimental spectra are represented by solid line. The fitted peaks are represented by open triangle	33
Figure 4.5: XPS spectra of CrAs _{0.40} Sb _{0.60} sample: (a) Cr2p core level spectrum, (b) As3d core level spectrum, (c) Sb3d core level spectrum. The experimental spectra are represented by solid line. The fitted peaks are represented by open triangle	35
Figure 4.6: XPS spectra of CrAs _{0.35} Sb _{0.65} sample: (a) Cr2p core level spectrum, (b) As3d core level spectrum, (c) Sb3d core level spectrum. The experimental spectra are represented by solid line. The fitted peaks are represented by open triangle.....	37
Figure 5.1: Resistivity versus temperature for CrAs under various hydrostatic pressure[1].	40
Figure 5.2: Transport measurement for CrAs sample.....	42
Figure 5.3: Derivative of the resistivity with respect to temperature	42

Figure 5.4: Transport measurement for CrAs _{0.55} Sb _{0.45} sample	43
Figure 5.5: Derivative of the resistivity with respect to temperature	43
Figure 5.6: Transport measurement for CrAs _{0.50} Sb _{0.50} sample	44
Figure 5.7: Derivative of the resistivity with respect to temperature	44
Figure 5.8: Transport measurement for CrAs _{0.45} Sb _{0.55} sample	45
Figure 5.9: Derivative of the resistivity with respect to temperature	45
Figure 5.10: Transport measurement for CrAs _{0.40} Sb _{0.60} sample	46
Figure 5.11: Derivative of the resistivity with respect to temperature	46
Figure 5.12: Resistivity versus temperature for CrAs _{1-x} Sb _x with concentration x=0.00, 0.45 and 0.50.	47
Figure 5.13: phase digram of CrAs as in [1].....	48
Figure 5.14 Antiferromagnetic transition Temperature in (K) versus Sb x(%) in CrAs _{1-x} Sb _x and versus applied pressure on CrAs as in[1]	49

ABSTRACT

Full Name : Mohammed Abdallah Khalid Abubaker
Thesis Title : Substitution effects in CrAs superconductor
Major Field : Physics Department
Date of Degree : December, 2015

Recently the effects of the external pressure on a single crystal of CrAs have been reported[1]. High pressure ~ 8 kbar was found to suppress both structural and antiferromagnetic transition temperatures. This behavior is accompanied with emergence of superconductivity near ~ 2 K [1]. In this thesis work, we investigate another tuning parameter (elemental substitution at the arsenic site, Sb in this work) in an effort to suppress both magnetic and structural transformation in CrAs compound. Resistivity measurements performed on $\text{CrAs}_{1-x}\text{Sb}_x$ have been used to obtain magnetic and structural transition temperature. We found that CrAs undergoes antiferromagnetic and structure transition at $T_N=240$ K. Moreover, a similarity between the Sb substitution and pressure effects in suppressing the antiferromagnetic order in CrAs has been confirmed in this work, a sharp linear drop in T_N has been observed near $x = 0.45$ with slope ~ -10.67 K/x%. The chemical composition and valance states in $\text{CrAs}_{1-x}\text{Sb}_x$ samples were obtained using XPS. We found that the atomic ratios for Cr and Sb are in excellent agreement with nominal values. Unexpectedly, we found that the arsenic has higher atomic ratio than nominal. We ascribed this to segregation of arsenic to the surface of sample. Moreover, the valance states for the elements were unchanged upon varying the antimony concentration; the chemical sates for the elements are Cr^{+3} , As^{-3} and Sb^{-3} .

ملخص الرسالة

الاسم الكامل: محمد عبدالله خالد أبو بكر

عنوان الرسالة: دراسة تأثير الإحلال على مركب (CrAs)

التخصص: فيزياء

تاريخ الدرجة العلمية: 2015 , December

حديثاً (حزيران-2014) تم اكتشاف خاصية فرط الموصلية في مركب زرنيخ الكروم (CrAs) عند درجة حرارة انتقالية سجلت عند 2 كلفن. تحقق هذا الانتقال الطوري عند تطبيق ضغط ميكانيكي وصل الى 8 كيلو بار، علماً بأن هذا المركب لا يمتلك هذه الخاصية عند الضغط الجوي. كما صاحب تناقص في درجة الحرارة الانتقالية لكل من التغير في التركيب البلوري والحالة الانتيفرومغناطيسية.

قمنا في هذه الأطروحة دراسة تأثير إحلال عنصر الأنتيموني بدلا من الزرنيخ في هذه العينة $CrAs_{1-x}Sb_x$ في محاولة لإحداث تغير في سلوك هذه المادة مع التغير في درجة الحرارة مشابهاً لأثر الضغط على هذا المركب. قمنا بقياس المقاومة النوعية عند درجات حرارة مختلفة تتراوح ما بين 300 و4 كلفن والتركيب البلوري عند درجة 300 كلفن. وجدنا أن درجة حرارة التحول المغناطيسي للمادة (والتي تعرف بدرجة حرارة نيل) تقل مع زيادة نسبة الأنتيموني. وجدنا أنه عند زيادة تركيز الأنتيموني إلى $x=0.45$ فإن درجة حرارة نيل قلت الى حد كبير بمعدل يساوي $(\frac{10.67-x}{X\%})$ كلفن على نحو يشبه تماماً تأثير الضغط الميكانيكي على نفس المركب. كما وجدنا عند نفس التركيز حدث تغير في التركيب البلوري للعينة هذه أصبحت العينة لها التركيب البلوري السداسي . بناء على نتائج في درجات الحرارة الانتقالية –مغناطيسية، تركيبية وفرط الموصلية- تمكنا من وضع رسم الشكل البياني للطور لهذه المادة ($CrAs_{1-x}Sb_x$).

CHAPTER 1

INTRODUCTION

1.1 **Discovery of superconductivity**

Superconductivity was discovered by the Dutch Physicist Kamerlingh Onnes in 1911 when he was investigating the variation of resistivity of high purity mercury with temperature. Onnes found that the resistance of the mercury drops suddenly to almost zero near 4 K. The conductivity is very large; hence name "superconductivity"[2]. Soon after the discovery, various elements, compounds and alloys were found to have similar superconducting behavior[3]. First theoretical explanation for this phenomenon was introduced in 1957. Three physicists from University of Illinois ; John Bardeen, Leon Cooper and Robert Schrieffer came up with a theory based on electron-electron attractive interaction through phonon exchanged mechanism. The coupled electron pairs Known as cooper pairs. The theory explained several properties of the superconducting material such as occurrence of the energy gap and isotopes effects[4].

1.2 **Basic properties of superconductor**

There are two fundamental properties for superconductors; disappearance of resistivity below certain critical temperature Known as the superconducting transition temperature (T_c). Second; the diamagnetic response to an applied magnetic field and was discovered in 1933 by Meissner and Oschensfeld; it is commonly known Meissner effect. Below T_c ; the superconducting material behaves as perfect diamagnetic material. The superconducting material completely repels the applied magnetic field to the outside as long as the field is below some critical applied magnetic field (H_c). Moreover, this is

unique to the superconducting state and distinguishes superconductor from "perfect conductors". As the applied field increases above H_c , the applied field either destroys the superconducting state in type-I superconductor, or the magnetic field start penetrating the bulk of type-II superconductor material. The emerging state (in type-II) is a mixed state of normal and superconducting state. The penetrating field forms vortices with normal core; its radius is known as the coherence length. Inside the core, superconductivity is destroyed[2].

1.3 Literature review

superconductivity remained confined to low temperatures (~ 20 K) until a new discovery radically changed the way we look and investigate the superconducting materials. In 1986 Bednorz and Muler discovered superconductivity in ceramic material Ba-La-Cu-O with $T_c \sim 30$ K. The discovered Cu-based ceramic material is insulator at room temperature. Bednorz and Muler measured the variation of the resistance ; and to their surprise and everyone else, the resistance of sample dropped to zero at 30 K, much higher than any known superconducting material. Within few months superconductivity was discovered in $YBa_2Cu_3O_7$ with $T_c \sim 93$ K much higher the boiling temperature of liquid Nitrogen. This marked a new era in superconductivity, ceramics and research in material science. The new class of material marked the beginning of "high temperature superconductors"[5]. Superconductivity is believed to be confined to Cu-O planes (sheets) in these new materials giving rise to the popular names for these materials such as "the Cuprates" and "Cu-based superconductor". Moreover, these materials are non-conventional superconductors in a sense that they do not follow BCS theory as they have high transition temperature and relatively very large superconducting energy gap as

compared with BCS-type materials. Recently (2008); a new type of unconventional superconductor ($T_c = 26$ K) has been discovered by Hideo Hosono and his group[6]. The new superconducting materials $\text{La}[\text{O}_{1-x}\text{F}_x]\text{FeAs}$ with ($x=0.05-0.12$) do not have Copper in their structure; they have Iron (Fe) instead. The transition temperature soon raised to about 43K under applying external pressure of 4GPa on F-doped LaOFeAs superconductor[7]. In almost all conventional superconductors; Fe is known to kill superconductivity; however; in these new materials, Fe seems to play important role in stabilizing superconductivity. The new superconductors, commonly known “Iron-based superconductors” mainly consist of layers of FeAs or FeP. These materials may or may not contain oxygen in their structure; and has been classified so far as shown in Figure 1.1 in to four basic families or groups according to these layers[8]:

- a. 1111-type family ($\text{LaFeAsO}_{1-x}\text{F}_x$): typically given as RFeAsO ; it consists of two negatively charged layers of FeAs or FeP which are sandwiched by positively charged RO interlayer where R is lanthanide. RFeAsO does not show superconductivity if it is not doped with fluorine, while the RFePO is a superconductor at $T_c = 4$ K. In both cases, the superconductivity transition temperature T_c is increased by doping with fluorine[8]. The maximum transition temperature in this family reach 56 K for $\text{R}=\text{Sm}$.
- b. 122-type family (BaFe_2As_2): this family has two layers of FeAs or FeP which are sandwiched by interlayer of alkaline-earth metal like Ba and also has a critical temperature at 38 K [9].

- c. 111-type family (LiFeAs): it is composed of two layers of FeAs or FeP which are sandwiched by interlayer composed from alkaline-metal like Li which in this case has a critical temperature at 18 K[10] .
- d. 11-type family(FeSe) : This simplest family of iron based superconductor, two layer of FeSe has no interlayer in between and also has a critical temperature $T_c = 8$ K that can be increased by the pressure [8].

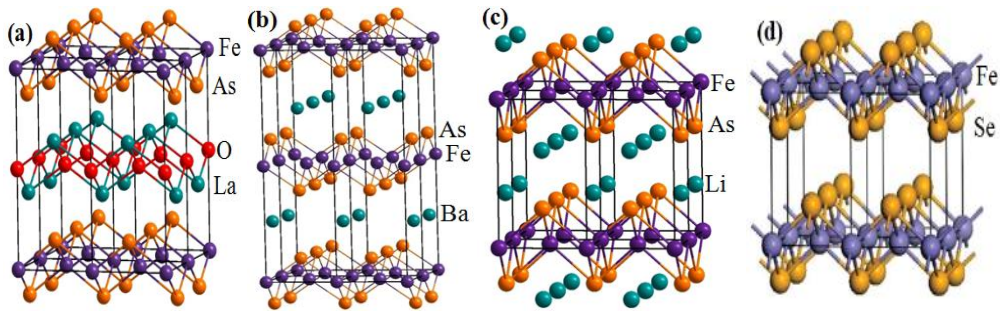


Figure 1.1: Family of iron based superconductor[8].

XPS properties for Fe-based superconductor were investigated in an effort to study its electron structure[11]. The variation of the binding energy of Fe2p and As3d core levels upon doping with fluorine in $\text{SmFeAsO}_{1-x}\text{F}_x$ superconductor were studied. No significant shift in the binding (less than 0.01eV) was found upon varying the concentration of fluorine from $x=0$ to 0.2[11].

Very recently, a new discovery in field has been found (Jun 2014); superconductivity has been discovered in CrAs by applying a high pressure. At ambient pressure, CrAs is non-superconductor[12]. CrAs belongs to large family of MX compounds where M is a transition metal and X could be P, As and Sb and has "commonly" orthorhombic structure[1]. Its magnetic transport and structural properties were studied extensively in the seventeenth and eighteenth of previous century in an effort to enhance the

semiconducting properties not superconducting[13]. It is well established that, CrAs undergoes first order antiferromagnetic transition at Neel temperature $T_N = 248$ K [14, 15], 260 K [16] and 280 K [13]. Furthermore, the transition temperatures of these states shifted to lower or higher temperature; with elemental substitution at the Arsenic sites in CrAs, commonly used elements with smaller atomic size such as Sulfur (S) and Phosphorus (P), or larger atomic size such as Selenium (Se) and Antimony (Sb). For example, Sulfur substitution in $\text{CrAs}_{0.92}\text{S}_{0.08}$ and $\text{CrAs}_{0.84}\text{S}_{0.16}$ lifted the Neel temperature; to temperature higher than room temperature; from $T_N = 260$ K to 320 K [17]. Similar trend was observed in Selenium (Se) in $\text{CrAs}_{0.80}\text{Se}_{0.20}$; T_N was reported to be at 600 K [18]. By contrast, most dramatic changes occurs when the smallest atomic size has been used; namely phosphorus. The Neel temperature (T_N) was dropped to 150 K in $\text{CrAs}_{0.92}\text{P}_{0.02}$ [19] and to 110 K in $\text{CrAs}_{0.97}\text{P}_{0.03}$ [20]. For higher P-substitutions, T_N was suppressed in $\text{CrAs}_{1-x}\text{P}_x$ with $x \geq 0.05$; at this concentrations of Phosphorus; no magnetic order was observed [20]. The decrease of T_N with x in $\text{CrAs}_{1-x}\text{P}_x$ was discussed by Kanay et al.[20] Kanay et al.[20], performed XRD measurements on $\text{CrAs}_{1-x}\text{P}_x$ with $x = 0.00, 0.03$ and 0.05 at temperature range 4.2 K and 300 K. They observed a significant change in lattice parameters as well as the volume of the lattice at 260 K for CrAs sample; the lattice parameter a and c increases abruptly, and b and v (unite cell volume) decreases abruptly as the temperature increases. They attribute these variations to antiferromagnetic phase transition[20]. Moreover, they observed as x increases to 0.03 the antiferromagnetic phase transition temperature T_N reduces to 110 K and larger contraction of lattice parameter b and the volume of the lattice were also observed[20]. Further increasing of phosphors, caused a disappearing of contraction in lattice parameter

b as well as the volume of the lattice, hence the magnetic ordering [20]. It is interesting to note that Kanaya et al. suggested applying a pressure on CrAs could suppress the Neel temperature and b lattice parameter in much a similar way to phosphorus substitution in $\text{CrAs}_{1-x}\text{P}_x$ [20]. Analogous results were observed in $\text{CrAs}_{1-x}\text{Sb}_x$ with intermediate concentration ($x = 0.40-0.50$). T_N was reduced to a minimum value at $T_N=150$ K in $\text{CrAs}_{0.50}\text{Sb}_{0.50}$. However, at $x < 0.40$ and $x > 0.50$ Sb-concentration, T_N increases to 320 K in $\text{CrAs}_{0.90}\text{Sb}_{0.10}$ and to 350 K in ($\text{CrAs}_{0.70}\text{Sb}_{0.30}$, $\text{CrAs}_{0.40}\text{Sb}_{0.60}$) and to 500 K in $\text{CrAs}_{0.20}\text{Sb}_{0.80}$ as shown in the phase diagram presented in Figure 1.2[21].

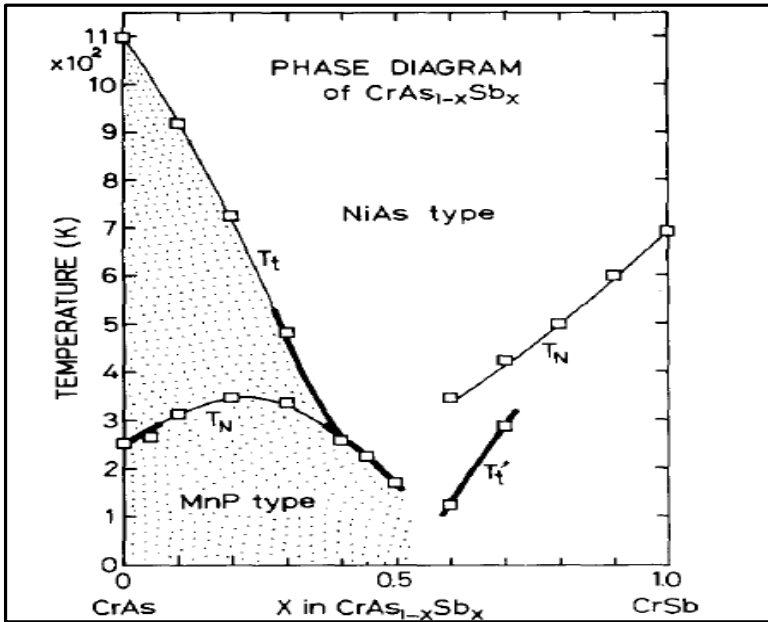


Figure 1.2: phase diagram of $\text{CrAs}_{1-x}\text{Sb}_x$ [21].

Structural transformation and magnetic properties have also been reported upon Cr site substitution with transition elements (T). It has been reported that, $\text{Cr}_{1-x}\text{T}_x\text{As}$ undergoes a structure transformation from orthorhombic to hexagonal structure for $T = \text{Mn}$ or Ti [22, 23]. Moreover, magnetic measurements showed CrAs has a helimagnetic structure below Neel temperature $T_N = 267$ K, Similar structure was observed in $\text{Cr}_{0.70}\text{Mn}_{0.30}\text{As}$ with Neel

temperature equal to 263 K. Higher Mn concentration as in $\text{Cr}_{0.40}\text{Mn}_{0.60}\text{As}$ caused the magnetic structure to become more sensitive to temperature variations. The material become ferromagnetic with Curie temperature close to 160 K, low spin state from 160 to 235 K, intermediate spin state from 235-700 K and a high spin state above 700 K[22].

None of the early studies on CrAs discussed the possibility of the presence of superconductivity state in CrAs system at low temperatures. Most of magnetic, structure and transport properties were investigated at temperature greater than 100 K. Very recently (June 2014); these properties have been investigated under high pressure and temperature range from 300 K to 2 K. It has been found, applying a high pressure on the CrAs has the similar effects as seen in Phosphors and Antimony substitution. Neel and the structure transition temperature have been simultaneously decreased by increasing the pressure and finally suppressed with a pressure value equal to 10 kbar. Surprisingly, at this critical pressure, superconductivity emerges with low transition temperature (~ 2.2 K) [1, 12, 24]. All magnetic, structural and superconducting characterization temperature for CrAs and how they affected with increasing pressure are illustrated in the temperature-pressure phase diagram shown in Figure 1.3 (below).

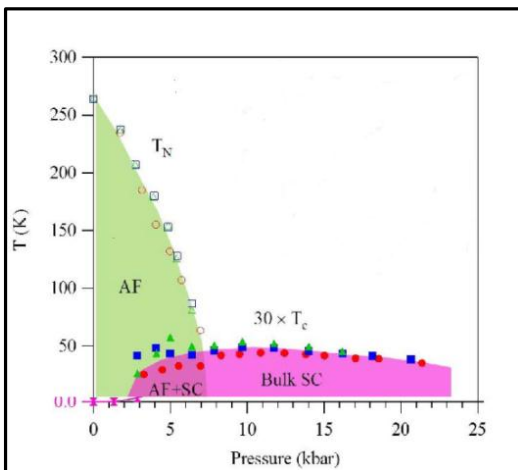


Figure 1.3: Phase diagram of CrAs [1].

The effects of pressure on FeAs have also been studied. By contrast, no similar behavior was found in FeAs; which remained non-superconductor under very high pressure (11.5GPa)[25]. More recently(February 2015) the superconductivity at $T_c=6.1$ K has been discovered in $K_2Cr_3As_3$ and also in $Rb_2Cr_3As_3$ with $T_c = 4.8$ K even without applying any pressure [26, 27]. The superconducting transition temperature has been confirmed in $K_2Cr_3As_3$ from magnetic dc susceptibility and transport measurements; it has been found the $K_2Cr_3As_3$ goes to diamagnetic state and its resistivity drops to zero below 6.1 K[28]. Moreover, the electrical resistivity of $K_2Cr_3As_3$ shows linear temperature dependence, which are very similar to the optimally doped cuprite superconductor and iron based superconductor; in which the resistivity of all these compounds follows with $\rho(T)=\rho_0+AT$ and is regarded as of non-fermi-liquid behavior[28]. All these findings point to the importance of this new Cr-based superconductor; which deserves more exploration of this Old-New compound. In this thesis work, we have investigated the effects of Sb substitution on the arsenic site on transport, structural and the magnetic properties of CrAs. Moreover, we have also investigated the effect of Sb substitution on oxidation state of the elements, using x-ray photoelectron spectroscopy (XPS) technique, for the first time to the best of our Knowledge. The XPS results Show no significant change in the oxidation state of the elements in the sample. We found that Sb substitution has similar effects like the external pressure on CrAs in suppressing both the structural and magnetic transition in this Cr-based superconductor in much similar way to what has been recently observed.

1.4 Thesis objective

The main objectives of this thesis work are the following:

1. To obtain the phase diagram of $\text{CrAs}_{1-x}\text{Sb}_x$, upon-Sb substitution.
2. To study the effects of Sb substitution on transport, magnetic and structural properties of CrAs. In particular we are looking for any similarities with applying external pressure in inducing superconducting state in CrAs, as has recently been discovered.
3. Examining the effects of Sb substitution on the oxidation state of the elements in $\text{CrAs}_{1-x}\text{Sb}_x$.

CHAPTER 2

EXPERIMENTAL METHOD

2.1 Preparation of CrAs_{1-x}Sb_x samples

Solid state reaction was used to prepare 12 samples of CrAs_{1-x}Sb_x with X = 0.00, 0.01, 0.05, 0.10, 0.15, 0.20, 0.45, 0.50, 0.55, 0.60, 0.65 and 1.00. High purity powders of Cr (4N), As (4N) and Sb (4N) with desired stoichiometric ratio were ground and mixed together by using agate mortar and pestle as exhibited in the Table 2.1 (below). The samples were pressed into pellets and sealed in an evacuated quartz ampoule partially filled with argon gas. The vacuum and Argon gas were needed to prevent the oxidation of constituent elements at high temperature during the solid state reaction. All samples were annealed by using programmable furnace. The annealing process is depicted in the Figure 2.1 (below). To avoid exploding the quartz tube, initially the temperature is raised to 600 °C just below the sublimation temperature of As (615°C) at the rate of 100 °C/ hr and remains at 600 °C for 10 hr before starts rising again to 1100 °C at the rate of 100 °C/ hr where samples were annealed for 24 hours. Then the temperature was reduced to 900 °C and was kept for 72 hr. Finally the samples were annealed at 300 °C for another 72 hr, and then quenched to room temperature.

Table 2.1 : Concentration of each constituent of CrAs_{1-x}Sb_x

<u>sample</u>	x	1-x	mwt(g/mole)	Cr (g)	As (g)	Sb (g)
<u>1</u>	0.00	1	126.918	0.4097	0.5903	0.0000
<u>2</u>	0.01	0.99	127.3864	0.4082	0.5823	0.0096
<u>3</u>	0.05	0.95	129.2599	0.4023	0.5506	0.0471
<u>4</u>	0.10	0.90	131.6018	0.3951	0.5124	0.0925
<u>5</u>	0.15	0.85	133.9437	0.3882	0.4755	0.1364
<u>6</u>	0.2	0.80	136.2856	0.3815	0.4398	0.1787
<u>7</u>	0.45	0.55	147.9951	0.3513	0.2784	0.3702
<u>8</u>	0.50	0.50	150.337	0.3459	0.2492	0.4050
<u>9</u>	0.55	0.45	152.6789	0.3406	0.2208	0.4386
<u>10</u>	0.60	0.40	155.0208	0.3354	0.1933	0.4713
<u>11</u>	0.65	0.35	157.3627	0.3304	0.1666	0.5029
<u>12</u>	1.00	0.00	173.756	0.2992	0.0000	0.7008

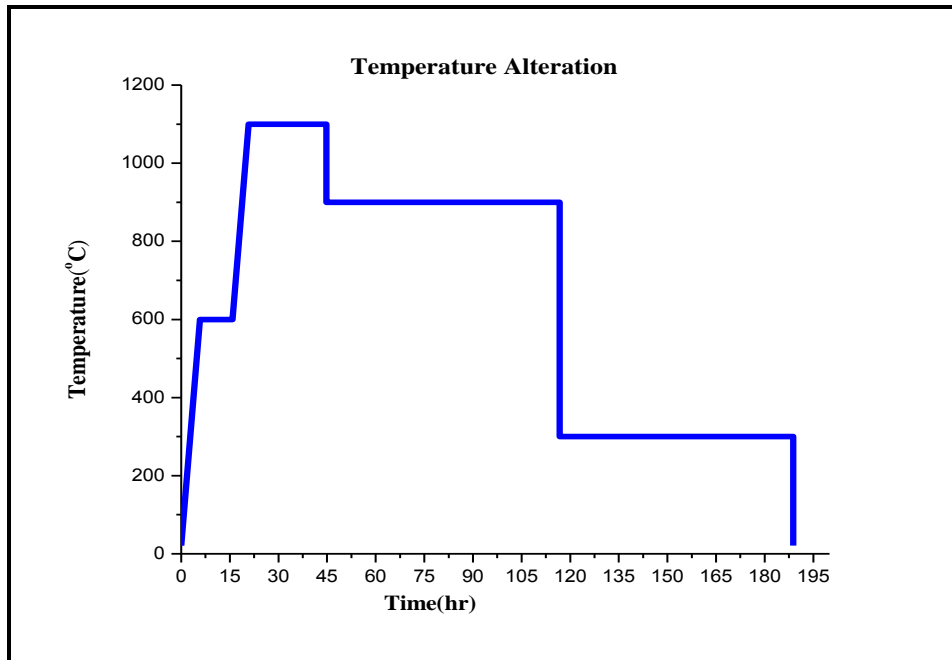


Figure 2.1: Platform step of the furnace for 12 samples of $\text{CrAs}_{1-x}\text{Sb}_x$

2.2 Characterization of the prepared samples

The prepared samples were characterized using the following techniques:

- a) Transport measurement using closed cycle refrigerator.
- b) X-ray diffraction analysis.
- c) X-ray photoelectron spectroscopy (XPS) measurement.
- d) Magnetic measurement.

2.2.1 Transport measurement using closed cycle refrigerator

The resistivity of each sample was measured in a temperature range 4-300 K using four probes technique, Cryostat (Model SHI-4T), vacuum mechanical pump, closed cycle refrigerator, temperature controller (Model #336), ac resistance (Model# LR-750). LABVIEW software has been used to control all measuring systems and collect the data. In this technique, samples were cut into a uniform bar shape then scraped to remove any

insulating oxide layer on the surface. Four probes connection points were made on the surface of sample using thin Copper wire and silver paste. The sample was securely mounted inside the Cryostat and it was connected with AC Resistance Bridge device (Model# LR-750) as shown in block diagram presented in the Figure 2.2. A four-wire AC Lock-Balance technique was used in LR-750 to measure the resistance of the sample. In this technique, 2 wires supply affixed amplitude of an Ac current at 16 Hz. The others two wires (middle wires) measure the resultant voltage across the sample and sends it back to the bridge to be balanced against an equal and opposite Ac voltage. This gives a continuous null signal at the front end amplifier of the bridges lock-Balance circuitry. Knowing the value of the equal and opposite Ac voltage gives the value of sample resistance. AC measurement method was utilized to measure the resistance of sample, because it has several advantages over the dc-method: it eliminates several problems associated with contact resistance, charges accumulation and capacitance effects- (capacitance that may arise from thin oxide layer between the terminals and the surface of the sample). Cryostat that houses the closed cycle refrigerator has to be pumped out to about 10^{-6} mbar for optimum operation and temperature stabilization. Closed Cycle refrigerator was used to cool the sample down to 4 K.

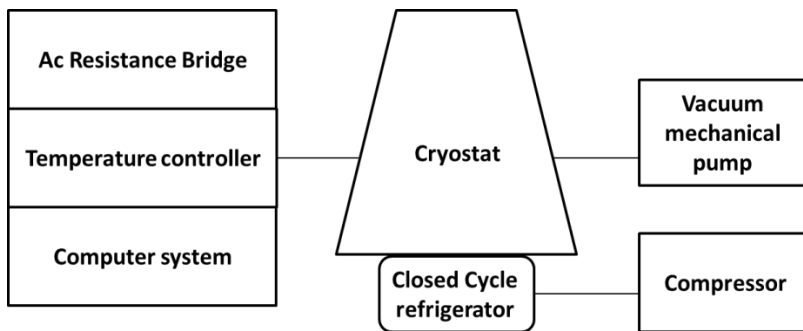


Figure 2.2: Schematic diagram of transport measurement (A.c set up)

2.2.2 X-ray diffraction analysis

X-ray diffraction analysis was performed on $\text{CrAs}_{1-x}\text{Sb}_x$ polycrystalline samples by using computerized Rigaku XRD (Model # MiniFlex600). In this technique, the powdered samples were packed on a silica glass and fixed on stage inside the Rigaku machine. All powdered samples were irradiated with monochromatic Cu K_α x-rays (600 Watt). The diffracted x-ray beams that coming from the sample were detected by standard scintillation counter at different angles from 10° to 80° . The angle was controlled by computer system and programmed to change with a rate $2^\circ/\text{mint}$. Silica glass holder was chosen because it does not have any x-ray diffracted peaks that overlap with peaks coming from the studied samples. The graph of the intensity against 2Θ was obtain and plotted for each sample. Maud software was used to analyze the data. The possible phases of the peaks were defined; Lattice parameter and the structure for each sample were also determined by using Maud program.

2.2.3 X-ray photoelectron spectroscopy (XPS) measurement

The XPS analysis was performed using a Thermo Scientific X-ray photoelectron spectrometer (Model # Escalab 250 Xi). The elemental composition and the oxidation state of all elements (Cr, As and Sb) in each sample were obtained by this technique. The experimental setup is shown in a schematic diagram presented in Figure 2.3. The XPS Spectrometer consists of ultra-high vacuum chamber fitted with several accessories: sputtering ion gun, X-ray source, electron energy analyzer, vacuum pumps and a low-energy electron (flood) gun. Each sample was fixed on a holder in the middle of the chamber. The surface of the sample was etched by argon ion beam focused on the surface of the sample by electrostatic lenses and used either for cleaning the surface of the

sample from contamination or depth profile analysis. All samples were irradiated with monochromatic Al K α x-rays (1486.6 eV) of spot size of diameter 650 μm by using X-ray source component. An incoming x-ray photon with energy $h\nu$ caused ejecting photoelectrons from the sample[29, 30]. The kinetic energy of these emitted photoelectrons was measured by the electron energy analyzer, which was operated in constant pass energy of 30 eV. The electron take off angle was 90° . The binding energy (BE) of the emitted electrons was calculated according to this equation $KE = h\nu - BE - \Phi$, which is based on the conservation of energy principle and only valid for photoelectrons that did not lose any energy when leaving the sample (elastic electrons)[30]. Analysis was performed under ultra-high vacuum with pressure in the 10^{-10} mbar range. The spectra were referenced to the adventitious carbon C1s peak at 284.6 eV. Avantage software was used for all data processing.

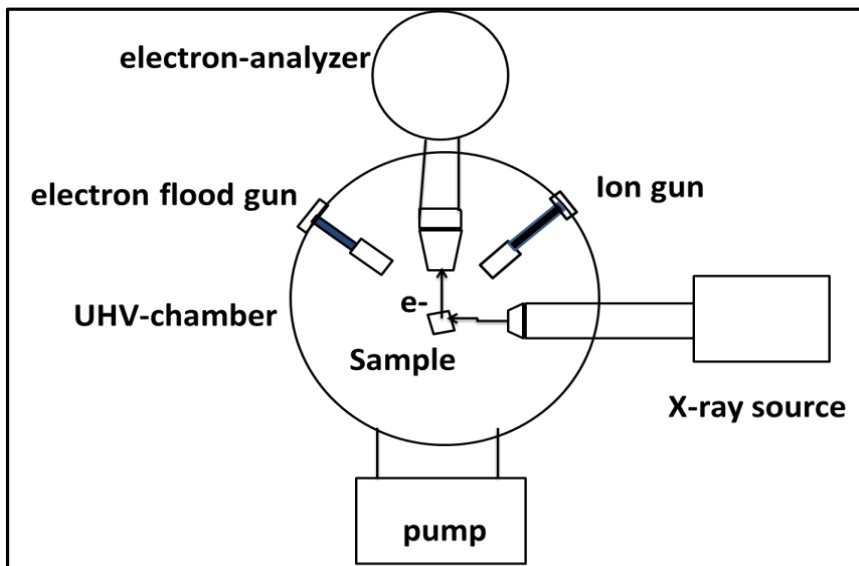


Figure 2.3: Schematic diagram of UHV chamber with other XPS components

CHAPTER 3

X-RAY DIFFERACTATION ANALYSIS

3.1 Result and discussion

X-ray diffraction patterns obtained for $\text{CrAs}_{1-x}\text{Sb}_x$ samples with $x = 0.00, 0.01, 0.05, 0.10, 0.15, 0.45, 0.55, 0.60, 0.65$ and 1.00 are shown in the following Figure 3.1- Figure 3.11.

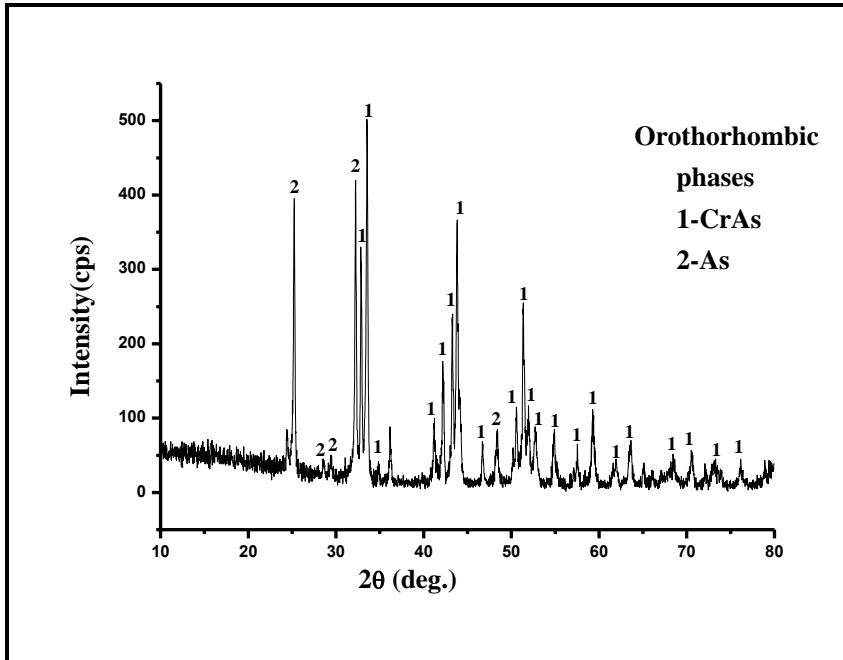


Figure 3.1: X-ray diffraction pattern of CrAs with the phases of the peaks

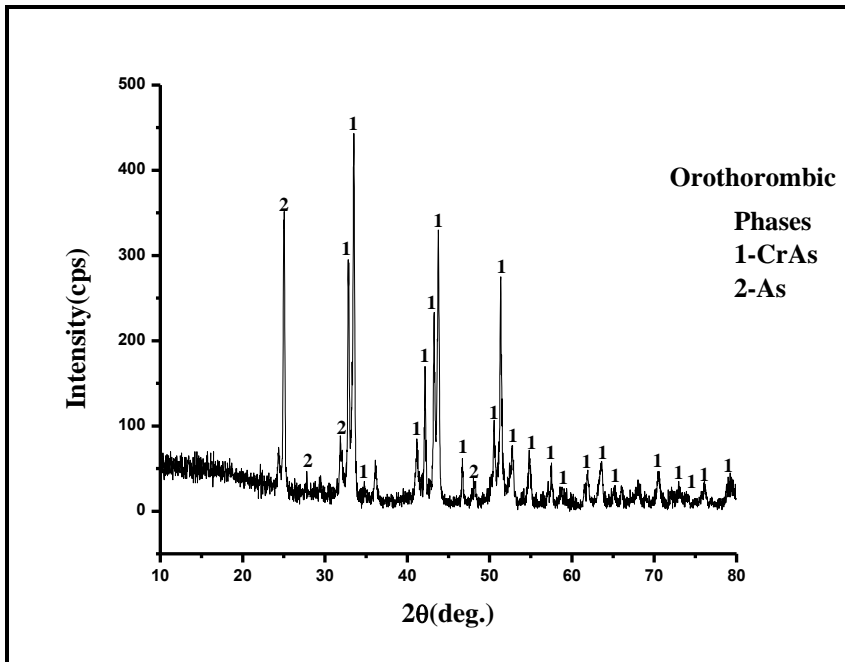


Figure 3.2: X-ray diffraction pattern of CrAs_{0.99}Sb_{0.01} with the phases of the peaks

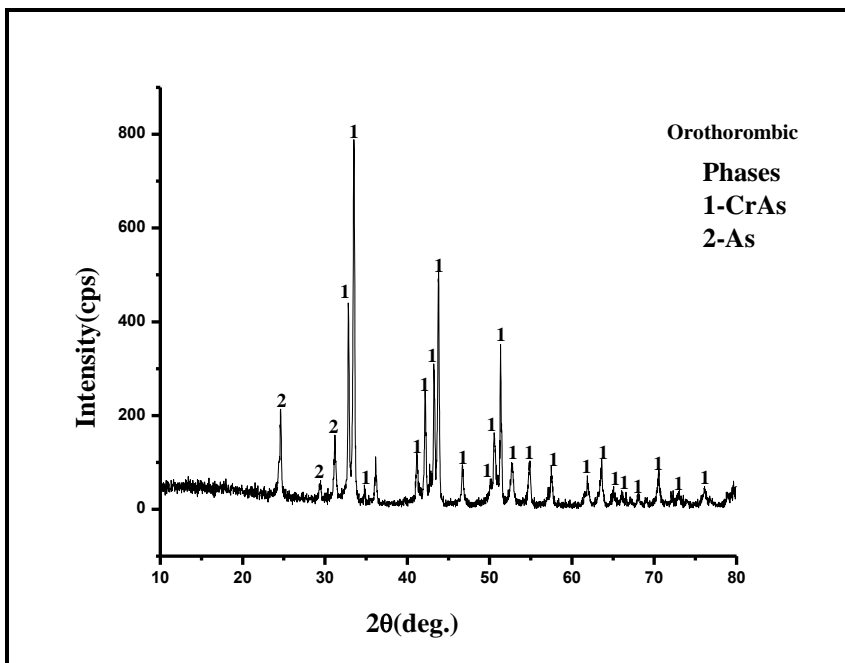


Figure 3.3: X-ray diffraction pattern of CrAs_{0.95}Sb_{0.05} with the phases of the peaks

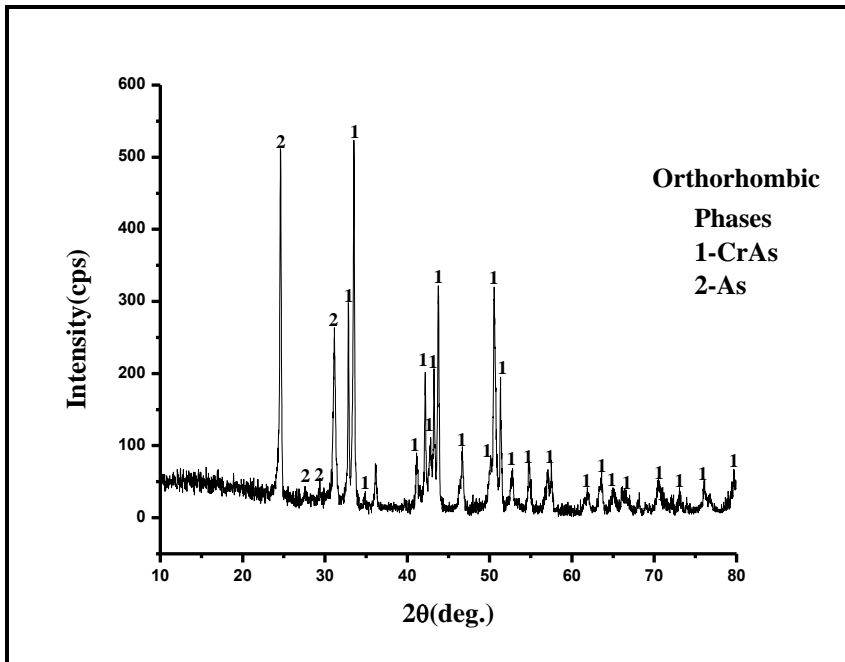


Figure 3.4: X-ray diffraction pattern of $\text{CrAs}_{0.90}\text{Sb}_{0.10}$ with the phases of the peaks

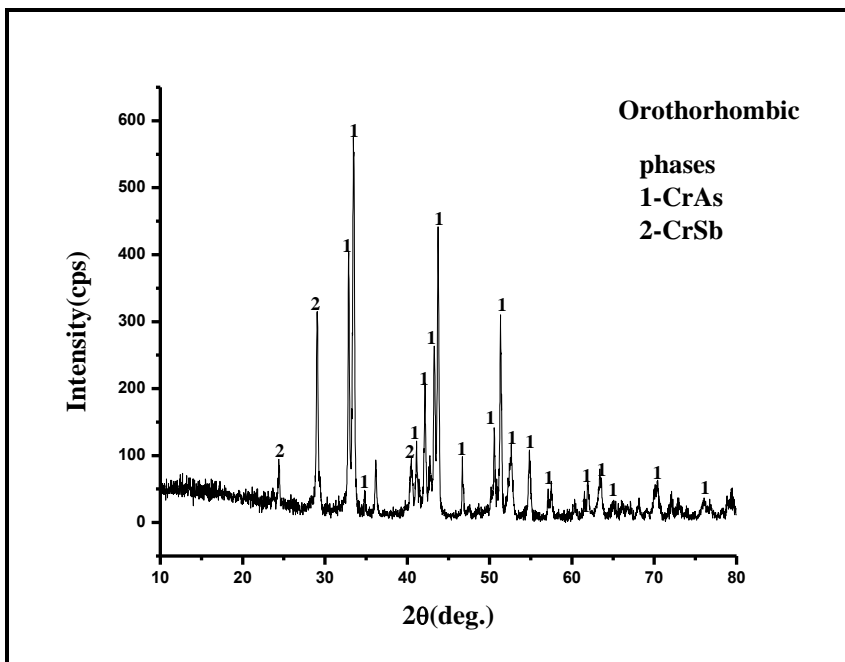


Figure 3.5: X-ray diffraction pattern of $\text{CrAs}_{0.85}\text{Sb}_{0.15}$ with the phases of the peaks

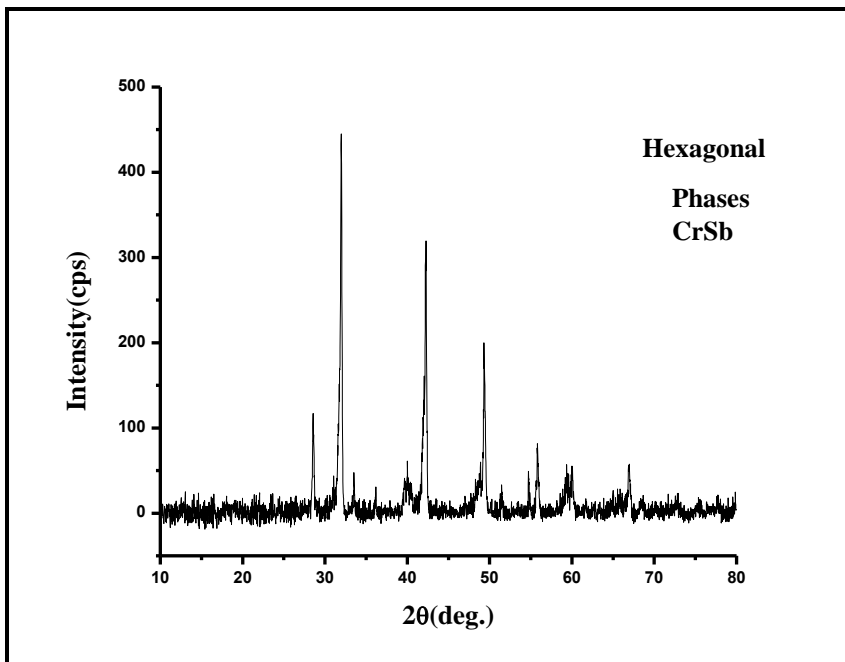


Figure 3.6: X-ray diffraction pattern of $\text{CrAs}_{0.55}\text{Sb}_{0.45}$ with the phases of the peaks

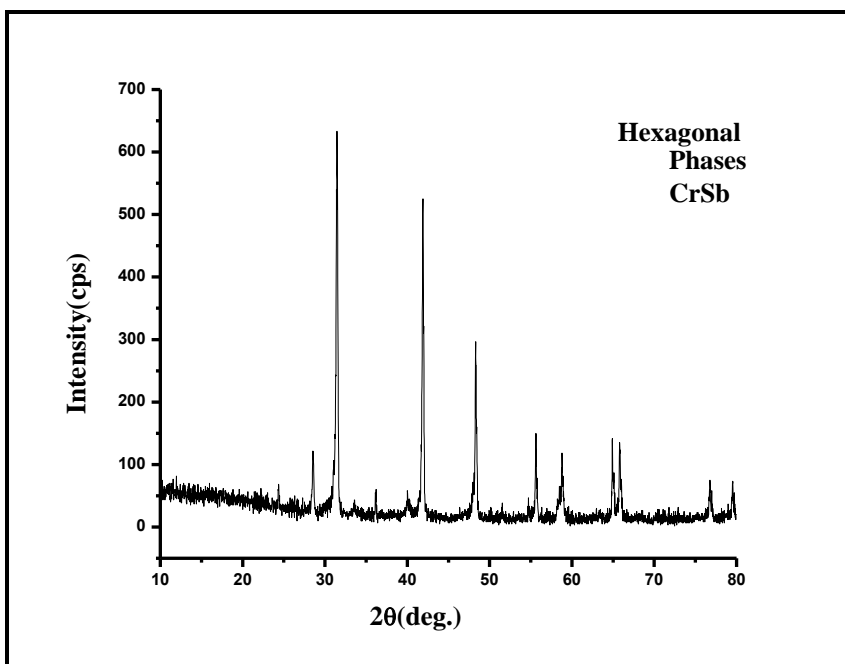


Figure 3.7: X-ray diffraction pattern of $\text{CrAs}_{0.50}\text{Sb}_{0.50}$ with the phases of the peaks

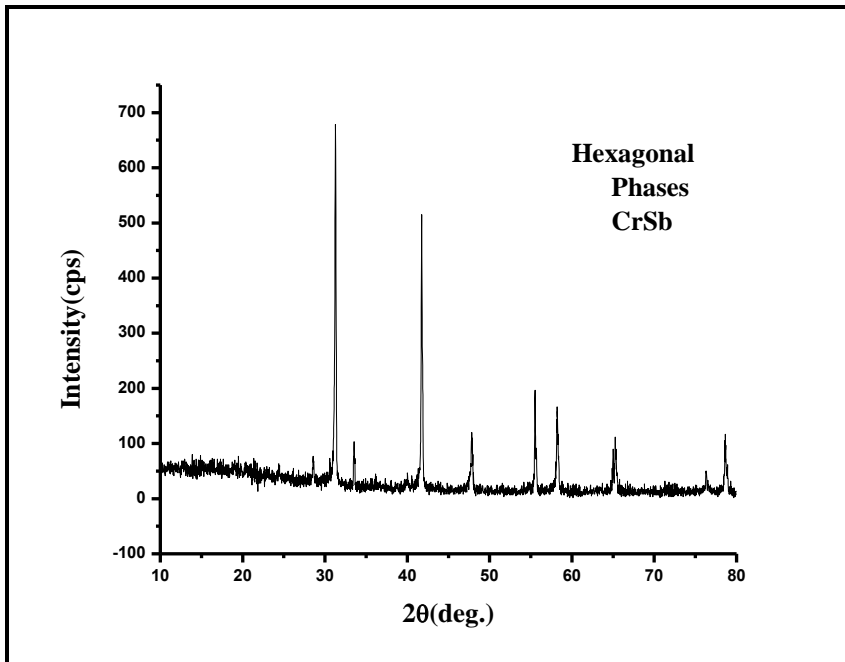


Figure 3.8: X-ray diffraction pattern of $\text{CrAs}_{0.45}\text{Sb}_{0.55}$ with the phases of the peaks

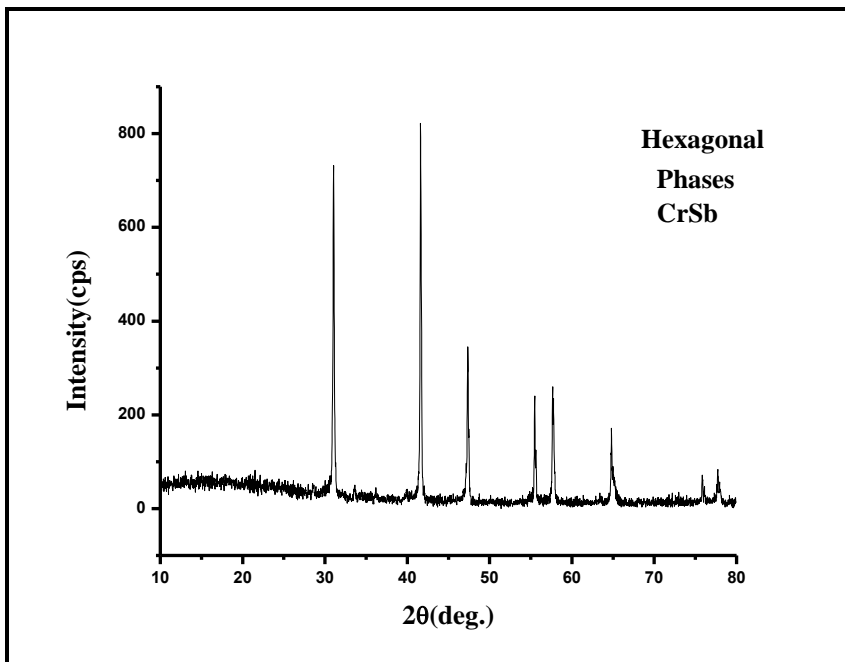


Figure 3.9: X-ray diffraction pattern of $\text{CrAs}_{0.40}\text{Sb}_{0.60}$ with the phases of the peaks

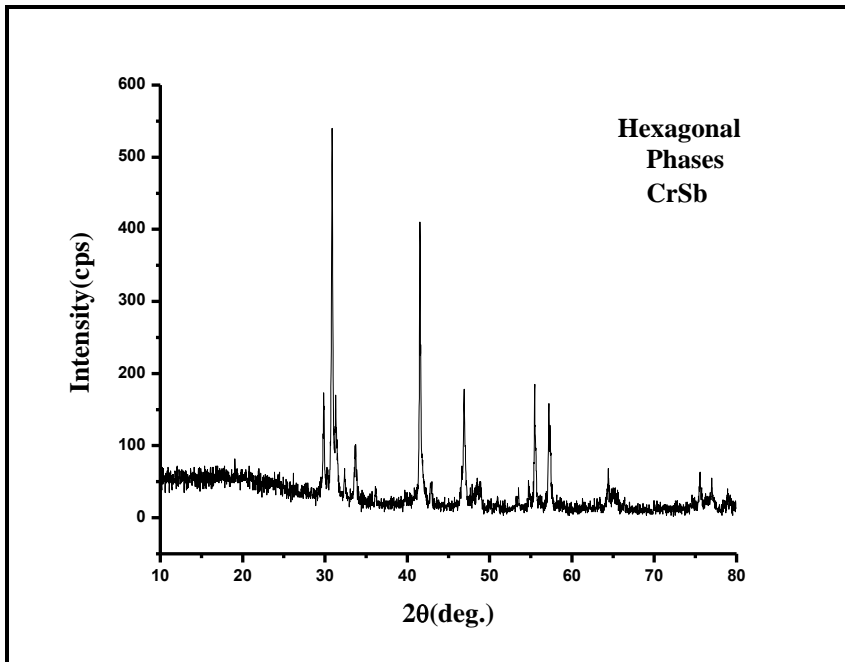


Figure 3.10: X-ray diffraction pattern of CrAs_{0.35}Sb_{0.65} with the phases of the peaks

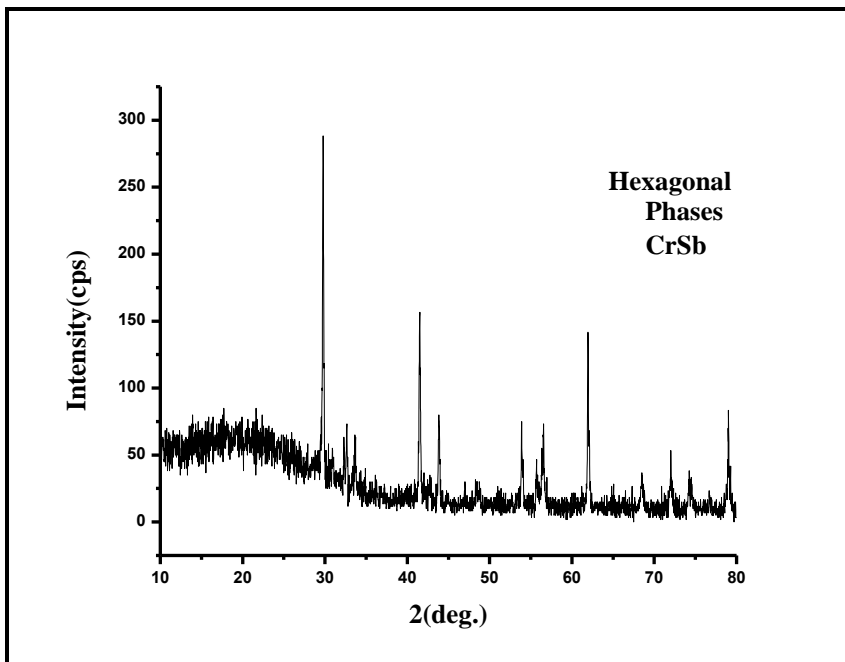


Figure 3.11: X-ray diffraction pattern of CrSb with the phases of the peaks

The variations in the patterns represented in Figure 3.1 to Figure 3.11 are a direct reflection of the effects of Sb substitutions on the structure of CrAs. The figures revealed that the orthorhombic structure dominates at low concentration of antimony; $x \leq 0.15$. At $x \geq 0.45$; the structure changed to hexagonal. The phases for all peaks as well as the structural parameters were determined in each sample by using Maud software. Table 3.1 and Figure 3.12 (below) reveal how the structural lattice parameters vary with antimony concentration in $\text{CrAs}_{1-x}\text{Sb}_x$ samples. It is interesting to note, at low concentration of antimony from 0% to 15%; the lattice parameter a, b and c are almost constant with x. But as the concentration of antimony increases from 15% to 45%, a significant change in lattice parameter a, b and c occurred. Moreover, the structure changed to hexagonal; both lattice parameters a and b shrink dramatically from (6.2066 Å, 5.6538 Å) to 3.6932 Å, respectively, while the lattice parameter c; elongates considerably from 3.4793 Å to 5.7651 Å. Upon further increase of the antimony concentration from 45% to 100%, a and b lattice parameters start increasing linearly. While c starts decreasing linearly. The composition dependence of the volume of unit cell is also shown in Figure 3.13. The unit cell volume v sharply decreases from large unit cell volume of the orthorhombic structure at $x=0.15$ to smaller unit cell volume of the hexagonal structure at $x=0.45$. Our results are consistent with initial studies on similar system reported by Kanaya et al. and Selte et al. [20, 31]. Similar behavior in the lattice parameters has been observed in CrAs doped with V and P. Kanaya et al. observed at low concentration of phosphorus in $\text{CrAs}_{1-x}\text{P}_x$ with $x=0.03$; the lattice parameter b and the volume of unit cell sharply decrease [20]. Similarly, this abrupt shrink in b lattice parameter was also observed in $\text{Cr}_{1-x}\text{V}_x\text{As}$ compound by Selte et al. at low value of x [31]. In contrast, a and c lattice parameters

have different pattern among the three compounds $\text{CrAs}_{1-x}\text{Sb}_x$, $\text{CrAs}_{1-x}\text{P}_x$ and $\text{Cr}_{1-x}\text{V}_x\text{As}$. In the case of $\text{Cr}_{1-x}\text{V}_x\text{As}$, a and c increase with x and their x dependence is opposite to these in $\text{CrAs}_{1-x}\text{P}_x$ [20]. Unlike $\text{CrAs}_{1-x}\text{Sb}_x$, no structure transformation was observed in $\text{CrAs}_{1-x}\text{P}_x$ upon varying the phosphorus concentration; the orthorhombic structure dominates at all phosphorus concentration. Only b has the same x dependence in all compounds $\text{CrAs}_{1-x}\text{Sb}_x$, $\text{CrAs}_{1-x}\text{P}_x$ and $\text{Cr}_{1-x}\text{V}_x\text{As}$. According to literature, the lattice parameter b is connected with occurrence of antiferromagnetic order in CrAs compound [16, 22, 32], It was found, at the Neel temperature, lattice parameters a and c increase suddenly, while b decreases abruptly as the temperature increases[20]. Moreover, Kanaya et al. observed the Neel temperature was shifted to lower temperature in $\text{CrAs}_{1-x}\text{P}_x$ in the region of low phosphorus concentration, where the rapid decreasing of b lattice parameter and the volume of unit cell are occurred. They ascribed this fall in Neel temperature to contraction of lattice parameter b as well the volume of lattice at these concentrations of phosphors. It is interesting to note that Kanaya et al. suggested applying a pressure on CrAs could suppress the Neel temperature and b lattice parameter in much a similar way to phosphorus substitution in $\text{CrAs}_{1-x}\text{P}_x$ [20]. Recently, Pressure effects on CrAs system have been studied by Wei Wan and his research group[1]. Wei Wan et al. found that applying a high pressure ~8 kbar on CrAs caused suppressing in structural and antiferromagnetic transition temperatures[1]. Moreover, they observed this suppressing is surprisingly accompanied with emergence of superconductivity at critical temperature $T_C = 2 \text{ K}$ [1].in this thesis, we found similar results in narrow range of Sb substitution in $\text{CrAs}_{1-x}\text{Sb}_x$ system; namely for $x = 0.45$, where the Neel temperatures was drastically

suppressed by about 150 K and the b lattice parameter and the volume of unit cell were abruptly decreased.

Table 3.1: Structural parameters of CrAs_{1-x}Sb_x samples

Sb%	a (Å)	b (Å)	c (Å)	structure
0	6.2082	5.6519	3.4691	Orthorhombic
1	6.2101	5.6569	3.4728	Orthorhombic
5	6.2114	5.6527	3.4707	Orthorhombic
10	6.2125	5.6536	3.4717	Orthorhombic
15	6.2066	5.6538	3.4793	Orthorhombic
45	3.6932	3.6932	5.7651	Hexagonal
50	3.7672	3.7672	5.7454	Hexagonal
55	3.8021	3.8021	5.7356	Hexagonal
60	3.8401	3.8401	5.7231	Hexagonal
65	3.8735	3.8735	5.7037	Hexagonal
100	4.1265	4.1265	5.4809	Hexagonal

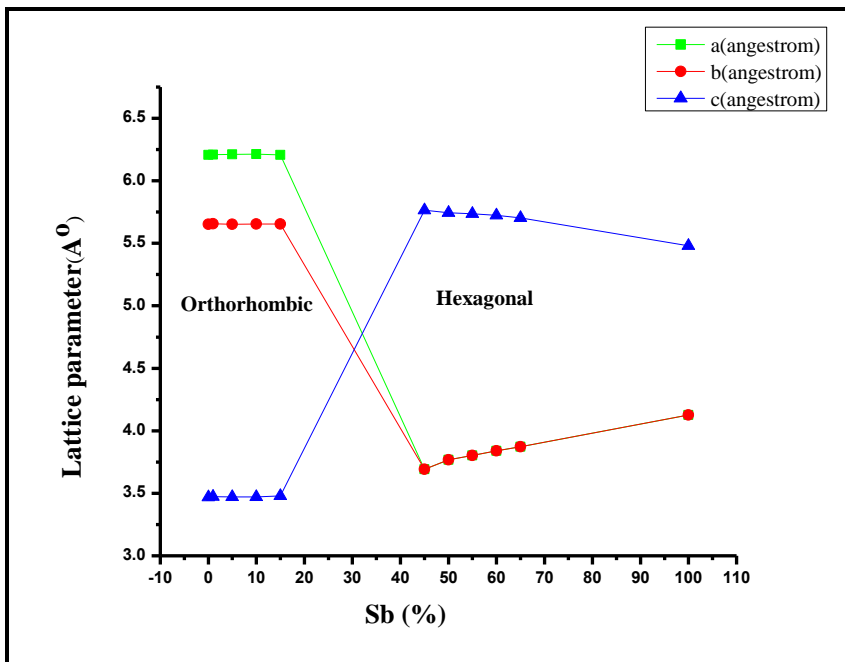


Figure 3.12: Variation of lattice parameters with the concentration of Sb in $\text{CrAs}_{1-x}\text{Sb}_x$

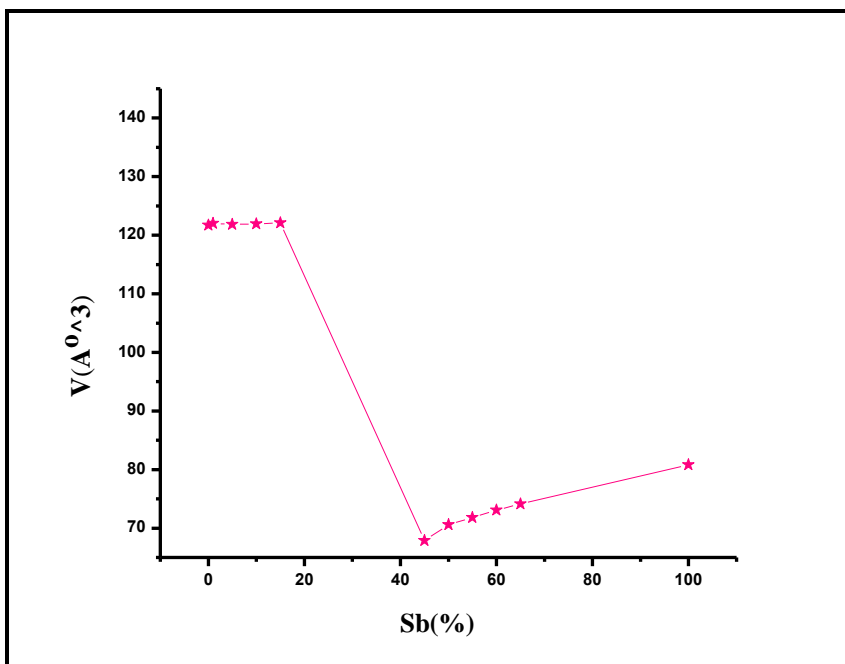


Figure 3.13: Variation of the volume of unit cell with the concentration of Sb in $\text{CrAs}_{1-x}\text{Sb}_x$

CHAPTER 4

X-RAY PHOTOELECTRON SPECTROSCOPY (XPS)

4.1 Introduction

X-ray photoelectron spectroscopy (XPS) is a surface and chemical analysis technique. It can be used to measure the elemental composition of a surface, uniformity of elemental composition across the surface and uniformity of elemental composition across the depth, oxidation state of each element within the surface, empirical formula of pure materials and elements that contaminate a surface [29]. This technique was developed in 1960 by Seighbahn and his research group and based on the famous photoelectric effect and the law of conservation of energy as shown in schematic diagram presented in Figure 4.1[29]. According to the photo electric effect; when a sample is exposed to an incident X-ray beam with high enough energy, which overcome the binding energy (BE) of the core electrons of the material in the sample, electrons are ejected from the sample and the extra energy of the incident x-ray beam shows up as kinetic energy (KE) of the emitted electrons[30]. The kinetic energies of the ejected photo electrons are measured by electron energy analyzer. By using conservation of energy, the binding energy of the emitted photo electrons can also be measured as in the following equation[33]:

$$\mathbf{BE = hf - (KE + \Phi)} \quad (4.1)$$

Where h is the plank constant, f is the frequency of incident x-ray photon, hf is the energy of the incident photon and Φ is the work function of the spectrometer. The obtained XPS spectra are displayed as intensity (electron yield) versus binding energy. Each element in the periodic table has its own and unique XPS peaks at characteristic binding energies. So from the binding energy values, we can identify each element in the sample as well its

oxidation state. Moreover, we can determine the elemental composition of each element on the surface of the sample from the intensity of the XPS peaks; the weighted intensity of the characteristic peaks is proportional to the concentration of the element within the surface of the sample[29].

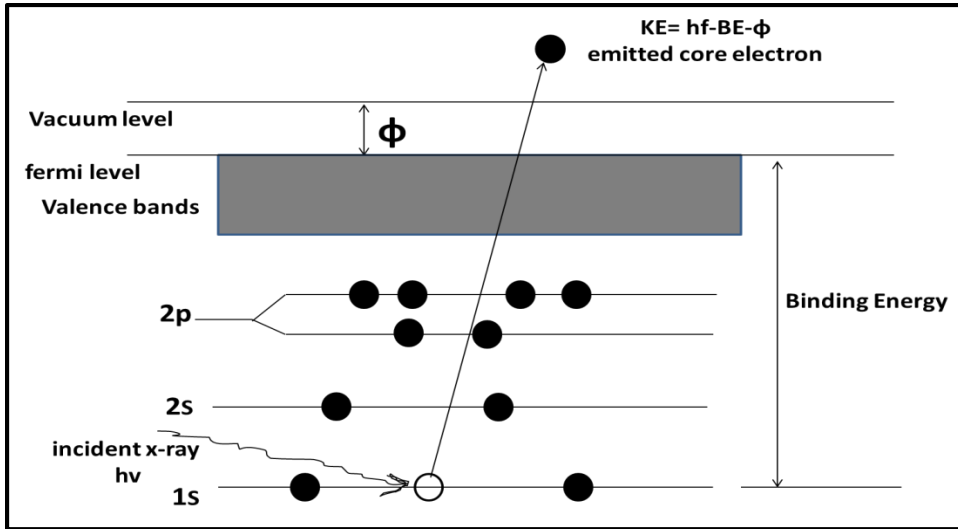


Figure 4.1: Schematic diagram of the basic principle used in XPS

4.2 Result and discussion

The chemical state and chemical composition of the $\text{CrAs}_{1-x}\text{Sb}_x$ samples were obtained using XPS. The spectra of all elements in each sample and deconvoluted peaks are shown in Figure 4.2 to Figure 4.6. We found that, chromium 2p core level spectrum shows multiplet splitting due to unpaired d electrons, in addition to spin-orbit splitting ($2p_{3/2}$ and $2p_{1/2}$). The binding energy for $\text{Cr}2p_{3/2}$ is assigned to alloy and the valence state is Cr^{+3} as reported in[34] . Similarly, arsenic and antimony 3d core level spectra also consist of spin-orbit doublets. The binding energy of $\text{As}3d_{5/2}$ is assigned to alloy and the valence state is As^{-3} as reported in [35]. In the case of antimony, there are two sets of doublets. The one with the high intensity is assigned to alloy and with valence state Sb^{-3}

as reported in [36, 37]. The Second set with the lower intensity is assigned to Sb_2O_3 [38]. The chemical composition of the samples was also determined using XPS. We found that the Cr and Sb atomic ratios agree with the nominal values as shown in Table 4.1. Unexpectedly, As composition is found higher than the nominal value. We ascribed this to the segregation of arsenic to the surface of the sample. The segregation of the arsenic to the surface of transition metal was investigated and confirmed for the first time using XPS technique by P. J. Godowski and his research group[39]. Godowski et al. [39] observed segregation of arsenic to the surface of iron bulk sample. Moreover, they deduced that the segregation of arsenic depends on the temperature at which the iron bulk sample was annealed [39]. They observed As segregates to the iron surface at 600 °C and become higher at 700 °C. Furthermore, they observed the segregation of phosphorous and sulfur to the surface of iron at 600 and 800 °C respectively[39].

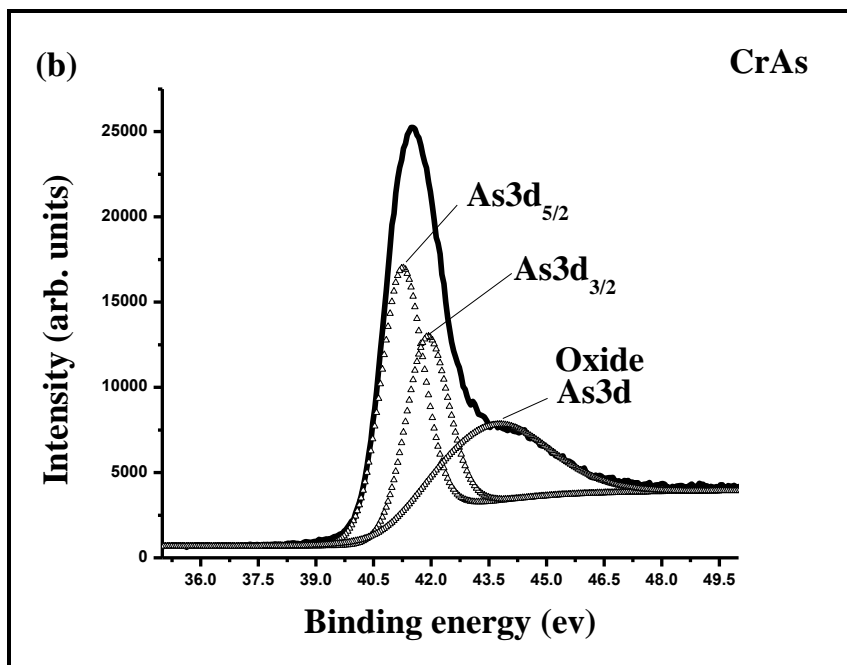
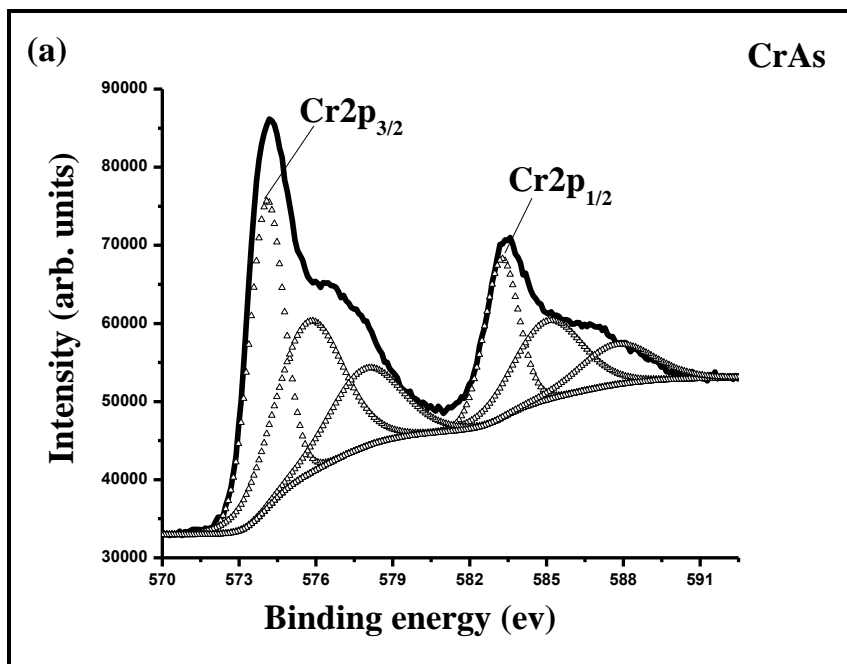
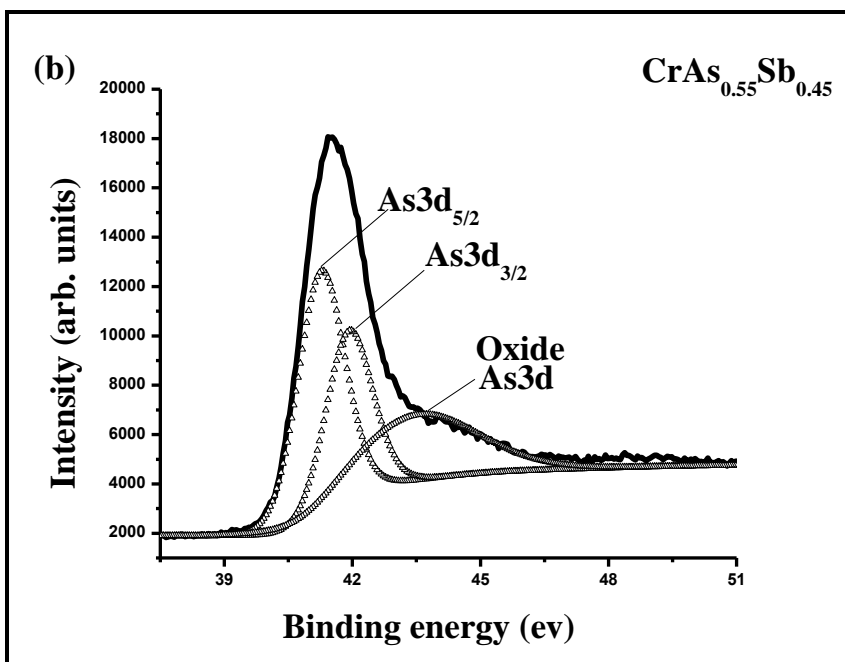
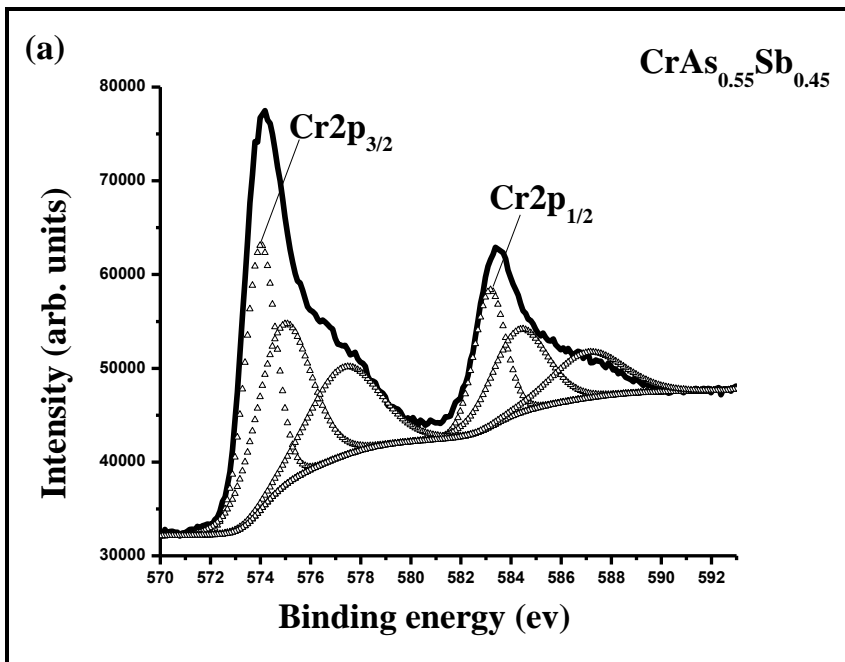


Figure 4.2: XPS spectra of CrAs sample: (a) Cr2p core level spectrum, (b) As3d core level spectrum. The experimental spectra are represented by solid line. The fitted peaks are represented by open triangle.



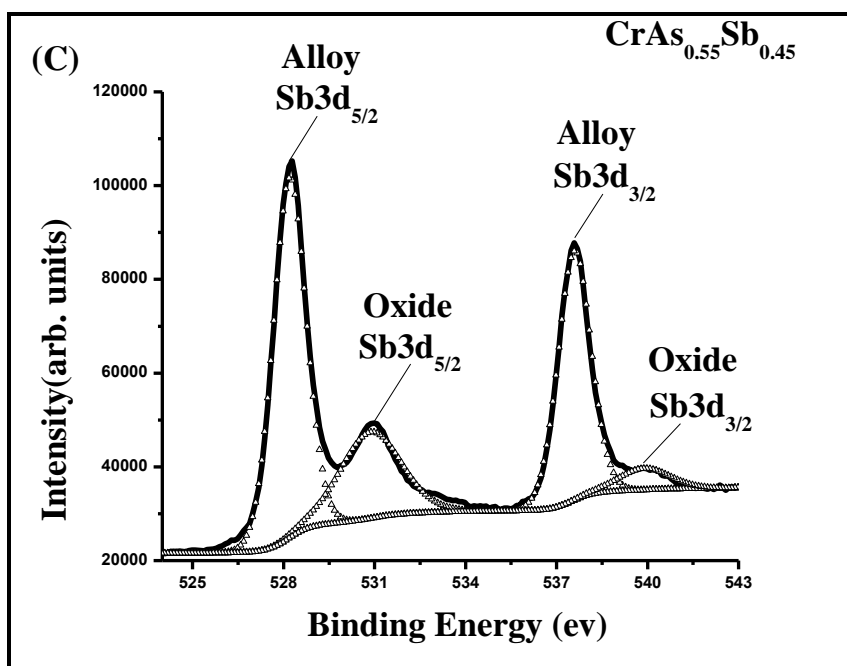
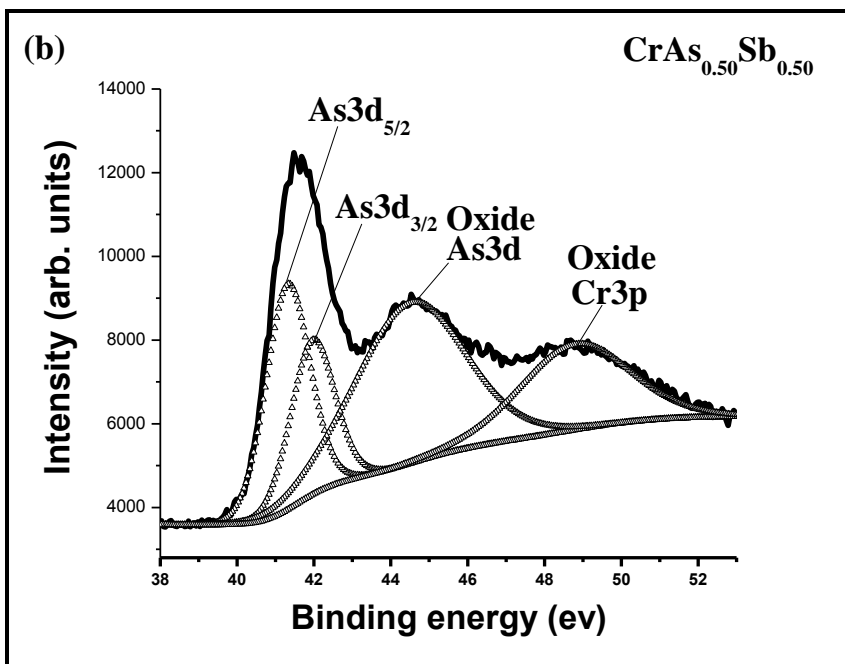
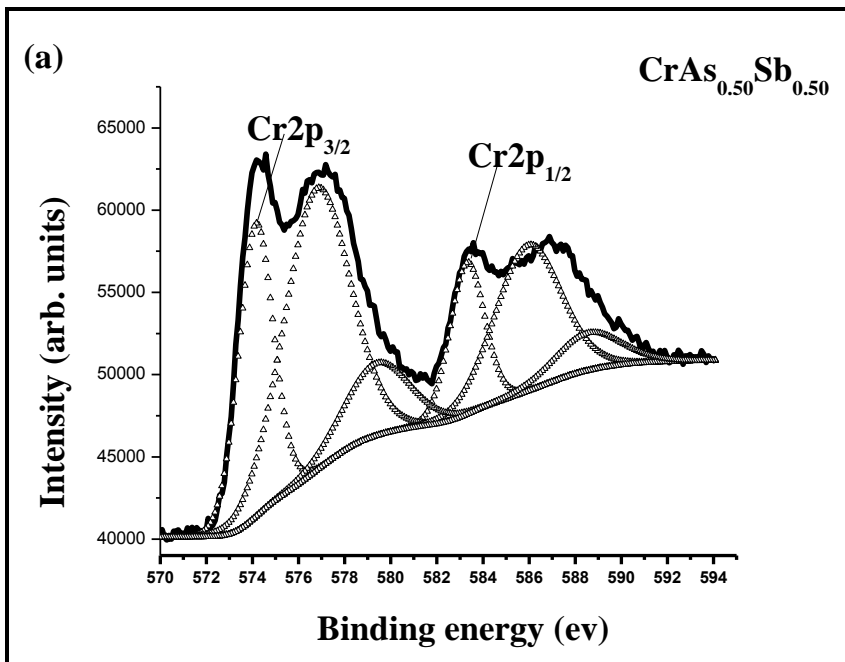


Figure 4.3: XPS spectra of $\text{CrAs}_{0.55}\text{Sb}_{0.45}$ sample: (a) Cr2p core level spectrum, (b) As3d core level spectrum, (c) Sb3d core level spectrum. The experimental spectra are represented by solid line. The fitted peaks are represented by open triangle.



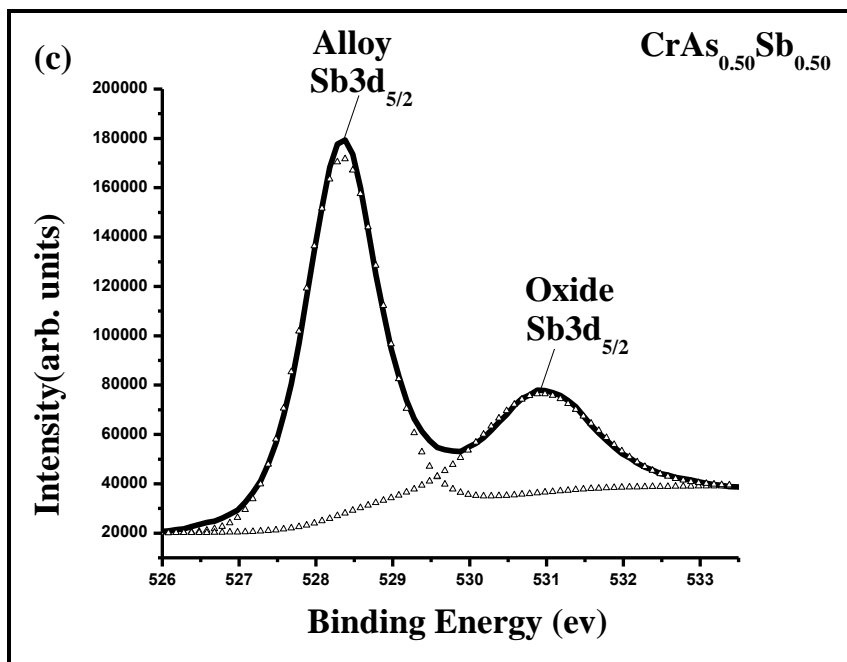
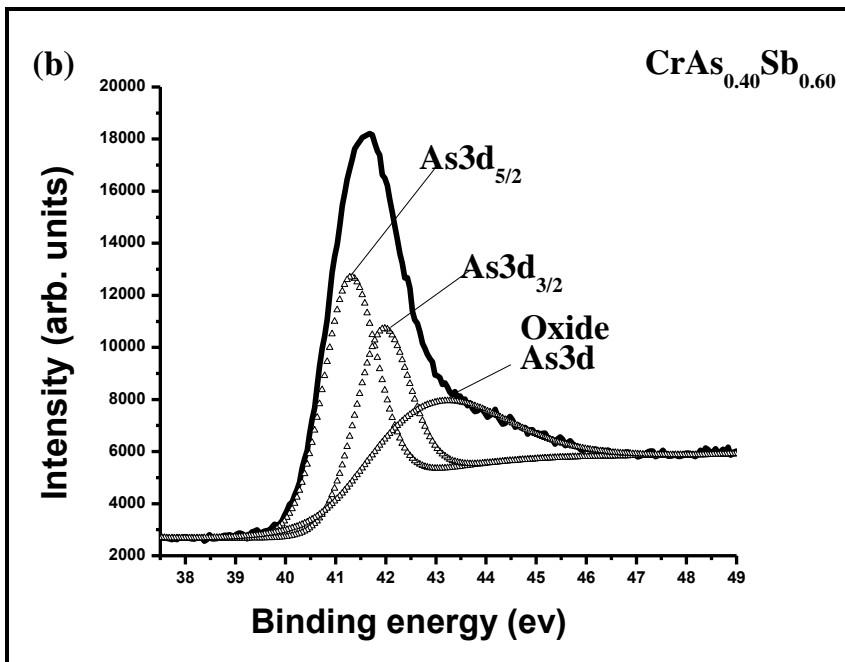
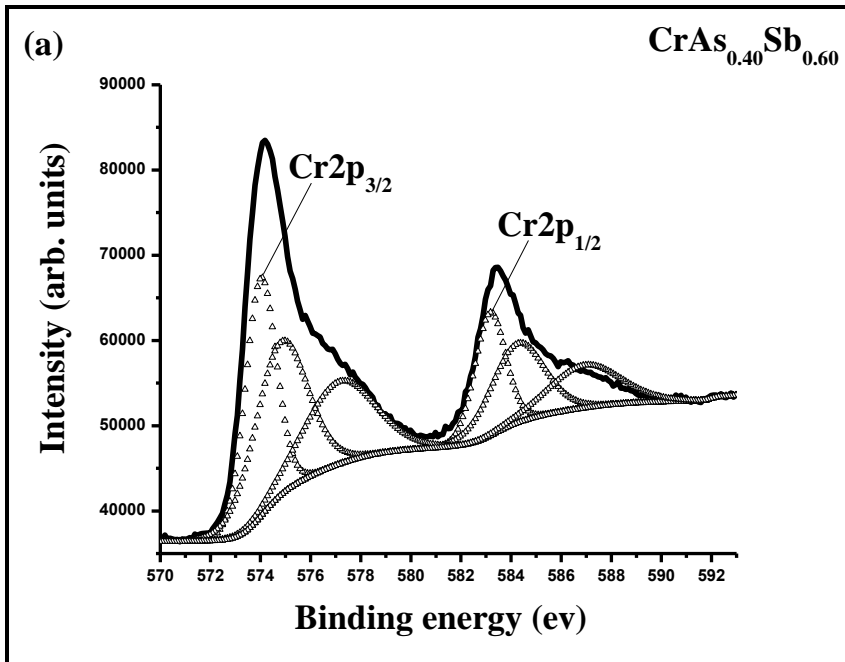


Figure 4.4: XPS spectra of $\text{CrAs}_{0.50}\text{Sb}_{0.50}$ sample: (a) Cr2p core level spectrum, (b) As3d core level spectrum, (c) Sb3d core level spectrum. The experimental spectra are represented by solid line. The fitted peaks are represented by open triangle



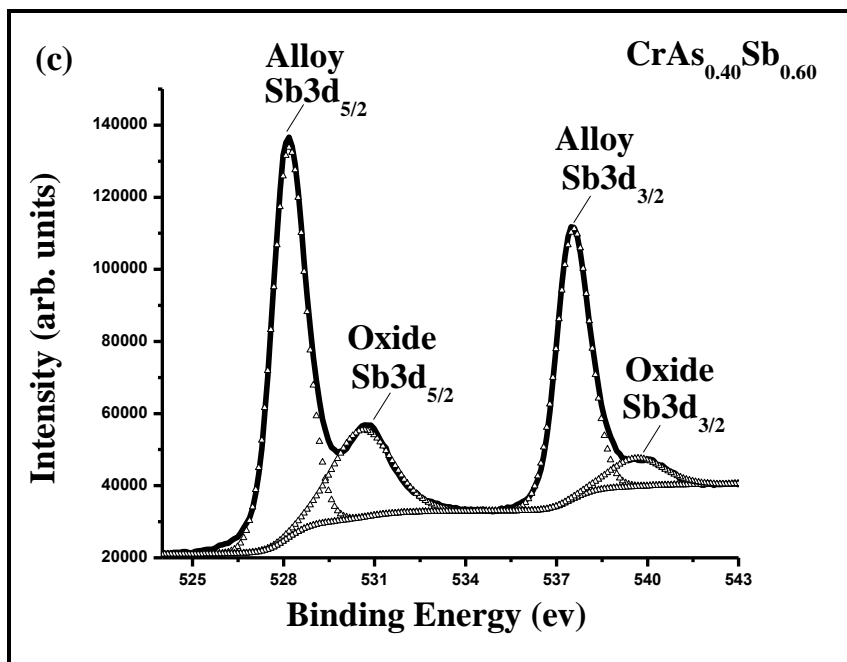
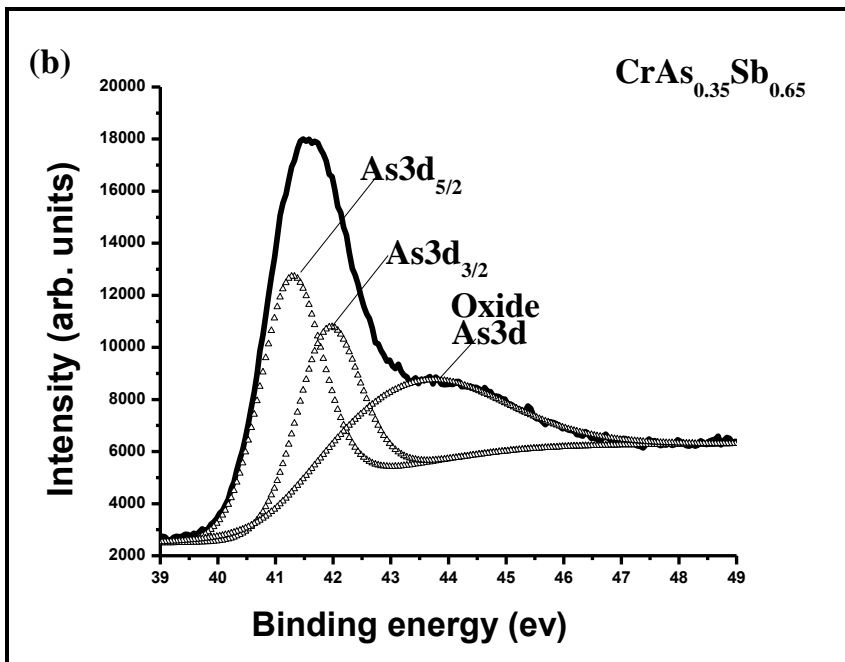
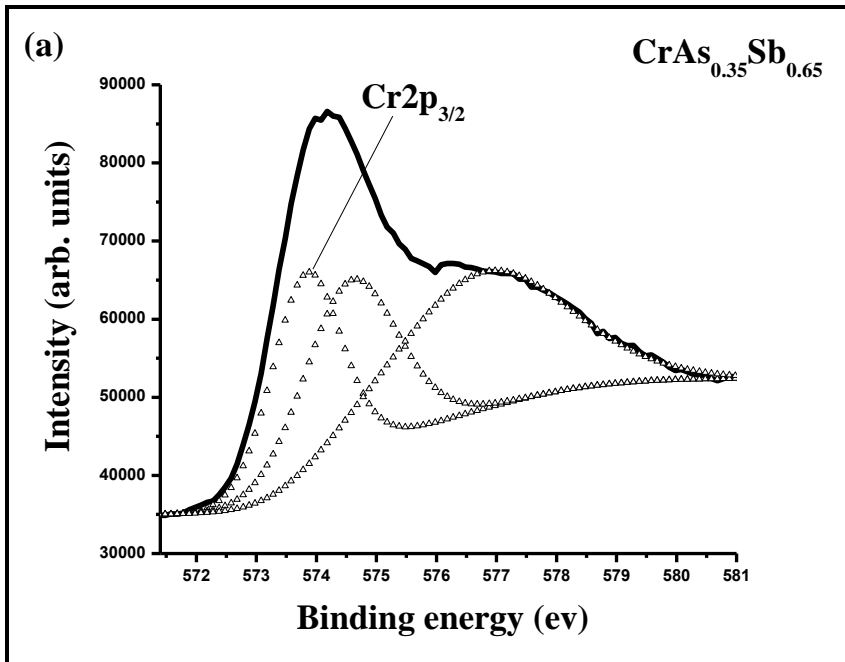


Figure 4.5: XPS spectra of $\text{CrAs}_{0.40}\text{Sb}_{0.60}$ sample: (a) Cr2p core level spectrum, (b) As3d core level spectrum, (c) Sb3d core level spectrum. The experimental spectra are represented by solid line. The fitted peaks are represented by open triangle



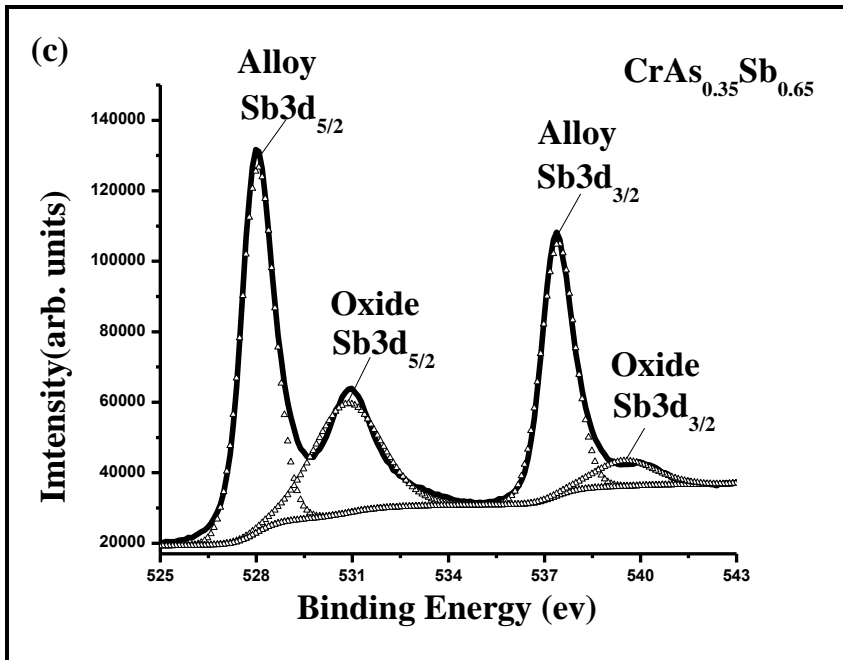


Figure 4.6: XPS spectra of CrAs_{0.35}Sb_{0.65} sample: (a) Cr2p core level spectrum, (b) As3d core level spectrum, (c) Sb3d core level spectrum. The experimental spectra are represented by solid line. The fitted peaks are represented by open triangle

Table 4.1: Summary of the XPS analysis for CrAs_{1-x}Sb_x samples

sample	Core Level	BE(ev) ± 0.2 ev	Oxidation state	Atomic ratio
CrAs	Cr2p _{3/2}	574.1	Cr ⁺³	1.00
	As3d _{5/2}	41.2	As ⁻³	0.83
CrAs _{0.55} Sb _{0.45}	Cr2p _{3/2}	574.0	Cr ⁺³	1.00
	As3d _{5/2}	41.3	As ⁻³	0.72
	Sb3d _{5/2}	528.2	Sb ⁻³	0.39
CrAs _{0.50} Sb _{0.50}	Cr2p _{3/2}	574.2	Cr ⁺³	1.00
	As3d _{5/2}	41.3	As ⁻³	0.46
	Sb3d _{5/2}	528.3	Sb ⁻³	0.45
CrAs _{0.40} Sb _{0.60}	Cr2p _{3/2}	574.0	Cr ⁺³	1.00
	As3d _{5/2}	41.3	As ⁻³	0.63
	Sb3d _{5/2}	528.2	Sb ⁻³	0.56
CrAs _{0.35} Sb _{0.65}	Cr2p _{3/2}	573.8	Cr ⁺³	1.00
	As3d _{5/2}	41.3	As ⁻³	0.84
	Sb3d _{5/2}	528.1	Sb ⁻³	0.65

CHAPTER 5

TRANSPORT MEASUREMENTS

5.1 Introduction

Resistivity measurements were performed on CrAs under various pressure values by W. Wei and his research group[1]. They observed at ambient pressure, an inflection point in the resistivity versus temperature curves at 264 K. They associated this behavior to antiferromagnetic (AF) phase transition[1]. Moreover, Wei W.et al.[1] , observed a shift in this phase transition to lower temperature as the pressure increases. As the AF-transition is completely suppressed, this is simultaneously associated with the emergence of superconductivity at critical pressure equal to 8 kbar and at a critical temperature $T_c = 2$ K. Their results are shown in the Figure 5.1. The arrows shown in Figure 5.1 indicate the antiferromagnetic phase transition temperature at the given applied pressure in kbar. These results strongly suggests a connection between the suppression of the antiferromagnetic order and emersion of superconductivity in CrAs compounds [12]. The question that arises in this regards, will element substitutions (Sb in this thesis) at the arsenic site be another tuning parameter in suppressing the AF-phase and eventually induces superconductivity in CrAs system? According to published literatures on $\text{CrAs}_{1-x}\text{Sb}_x$ [21], only intermediate concentration of the antimony in $\text{CrAs}_{1-x}\text{Sb}_x$ with x ranging between 0.40 to 0.50 has been found to reduce the antiferromagnetic transition temperature. This ultimately may induce superconductivity in CrAs.

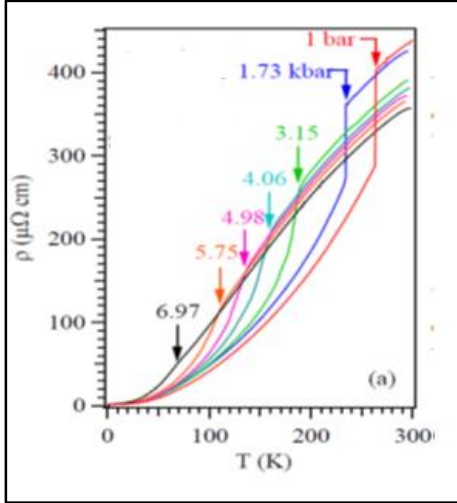


Figure 5.1: Resistivity versus temperature for CrAs under various hydrostatic pressure[1].

5.2 Result and discussion

The resistivity measurements for $\text{CrAs}_{1-x}\text{Sb}_x$ are presented in this section. In Figure 5.2 to Figure 5.12, we present the results $x = 0.00, 0.45, 0.50, 0.55$ and 0.60 . The measurements were performed during cooling and heating of the concerned samples in the temperature range (300-4) K. For $x = 0$, the resistivity curves clearly shows sharp drop at about 263 K for the heating curve and reveals a minimum at about 254 K. These transitions indicate a transition to antiferromagnetic state at low temperature. The transition temperatures have been obtained from the maximum/minimum in the derivative of the resistivity with respect to temperature. The derivatives of the resistivity for various Sb concentrations are shown in the Figures 5.3, 5.5, 5.7, 5.9, and 5.11. The resistivity curves clearly reveal an irreversible behavior during cooling and heating cycles (for example see Figure 5.2). This may be due to irreversible behavior in antiferromagnetic-paramagnetic transition, or temperature lag between the two protocols. Structural transition at low temperatures may also cause an increase in the density of defects, which may also cause some discrepancy

in the resistivity measurements (increase in resistivity). For $x = 0.0$, the antiferromagnetic transition temperature in the cooling process occurs at Neel temperature $T_N = 240$ K. At this temperature; the resistivity of CrAs shows maxima. The Neel temperature obtained during heating is $T_N = 263$ K. The resistivity curve followed different behavior at the transition temperature, revealing sharp jump at T_N . These results are in agreement with transport measurement carried out on single crystal of CrAs by H. Kotegawa and his research group[40], they associated this difference to micro cracks, which are formed in the CrAs due to irreversible change in the lattice parameter b at the antiferromagnetic transition temperature [40]. Therefore, we determined the antiferromagnetic transition temperature from resistivity versus temperature curves that obtained from resistivity measurements during cooling in order to avoid the effects of micro cracks. Moreover, superconducting transition in these doped polycrystalline samples have not been observed down to 4.0 K, the lowest temperature available in our system.

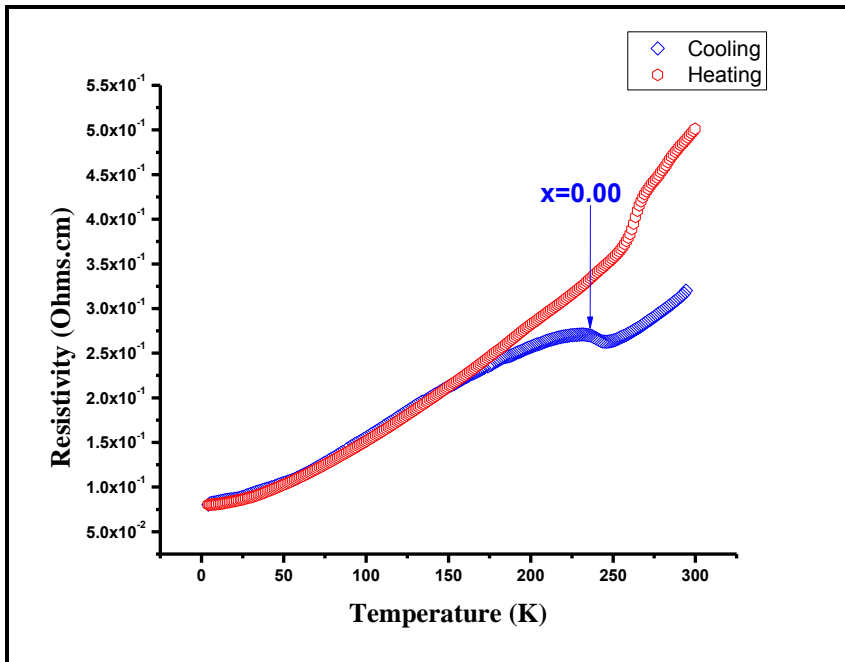


Figure 5.2: Transport measurement for CrAs sample

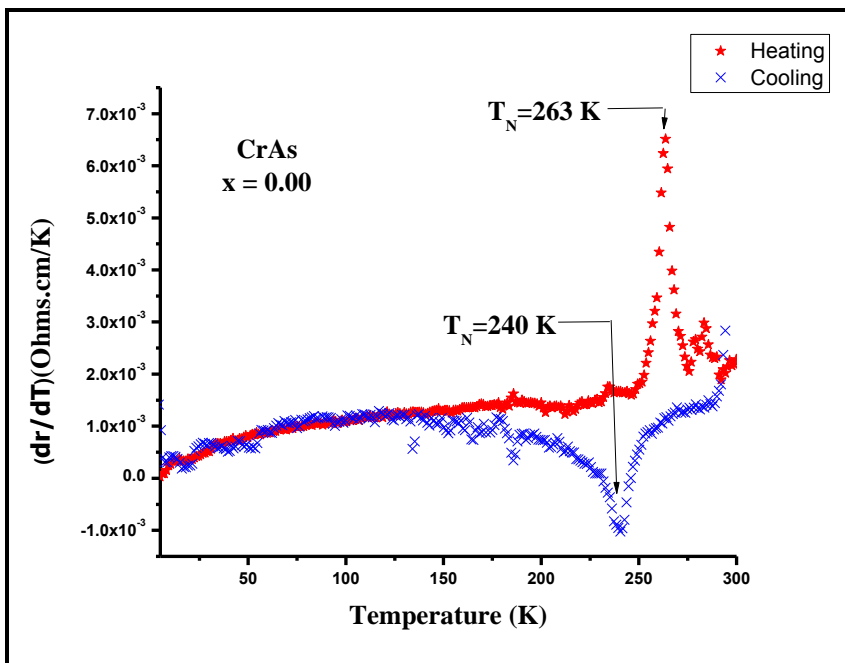


Figure 5.3: Derivative of the resistivity with respect to temperature

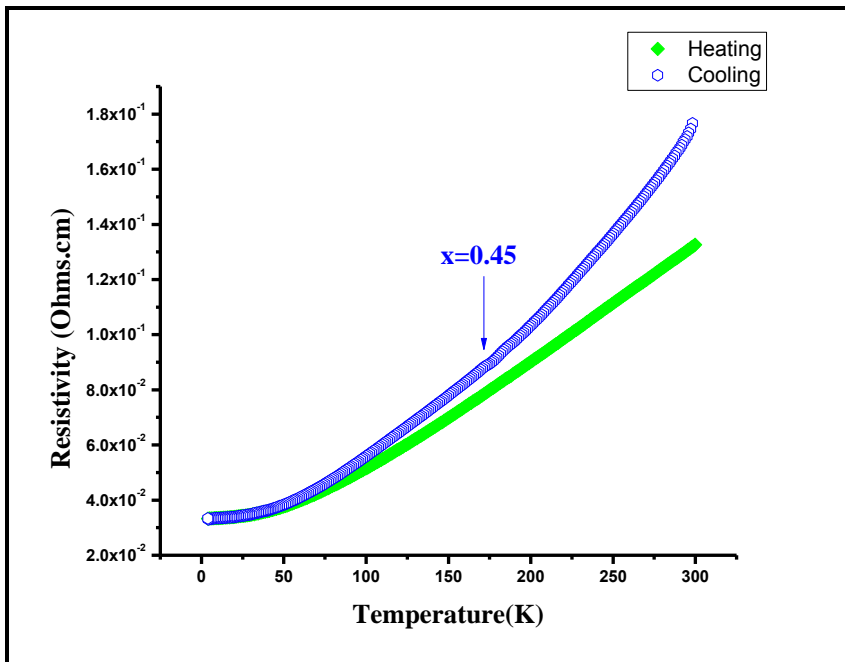


Figure 5.4: Transport measurement for $\text{CrAs}_{0.55}\text{Sb}_{0.45}$ sample

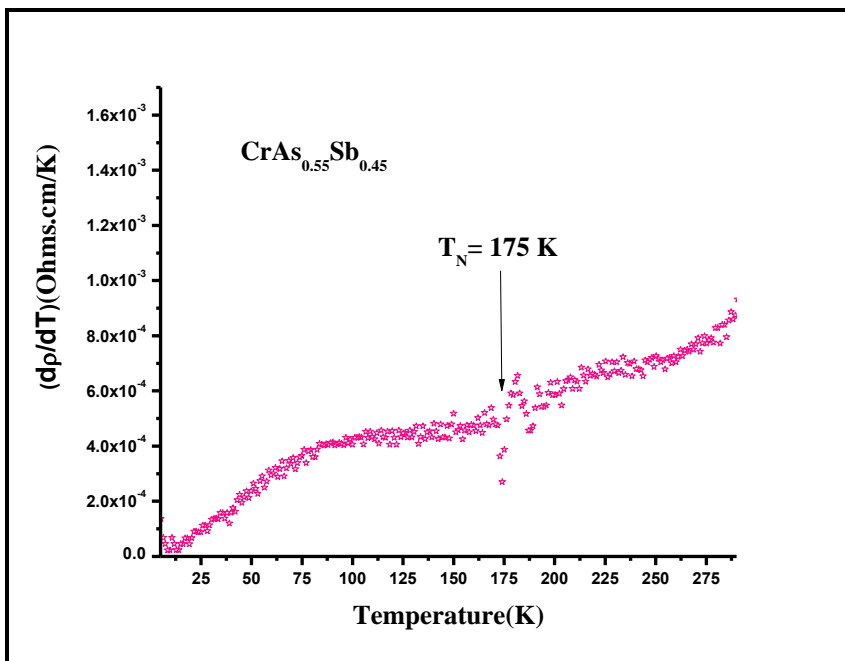


Figure 5.5: Derivative of the resistivity with respect to temperature

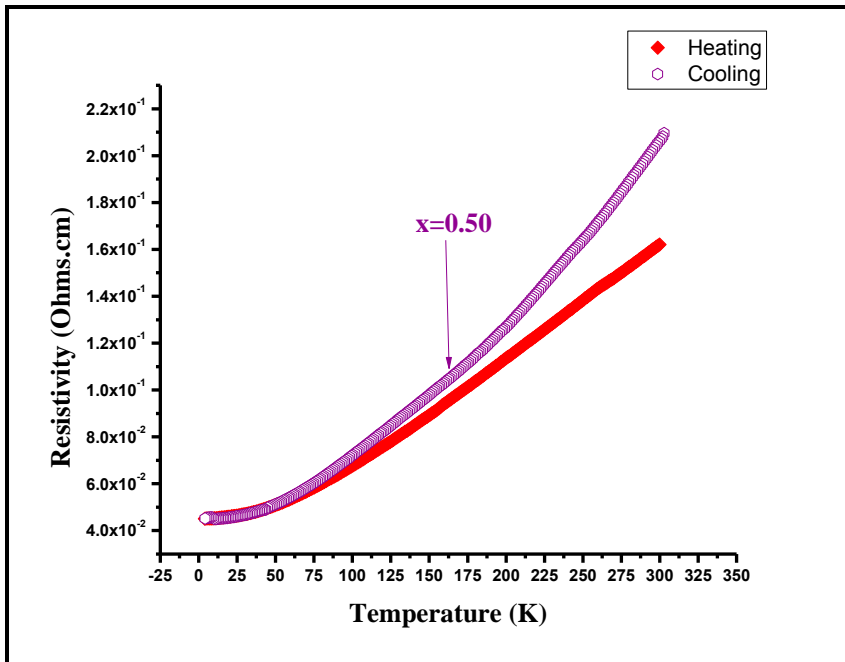


Figure 5.6: Transport measurement for $\text{CrAs}_{0.50}\text{Sb}_{0.50}$ sample

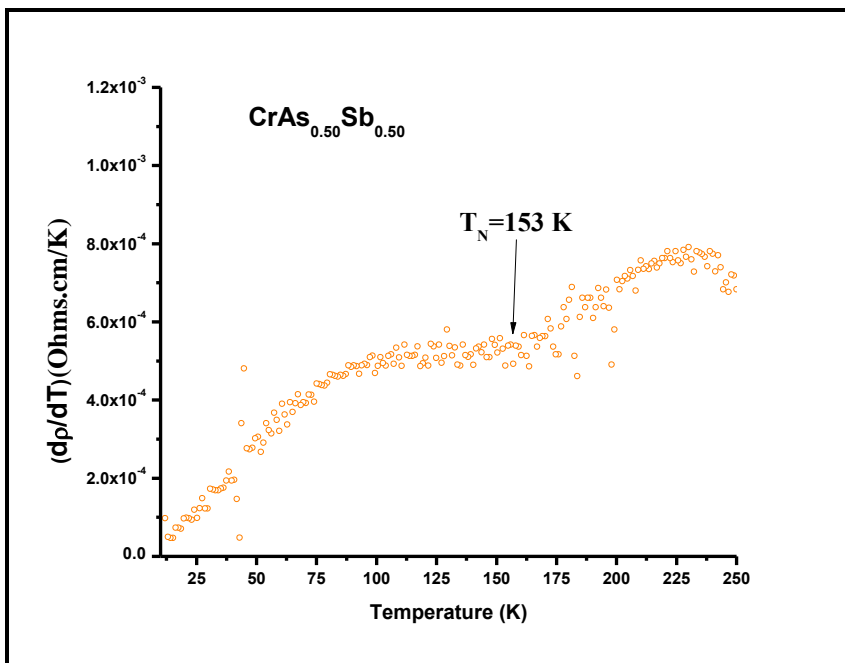


Figure 5.7: Derivative of the resistivity with respect to temperature

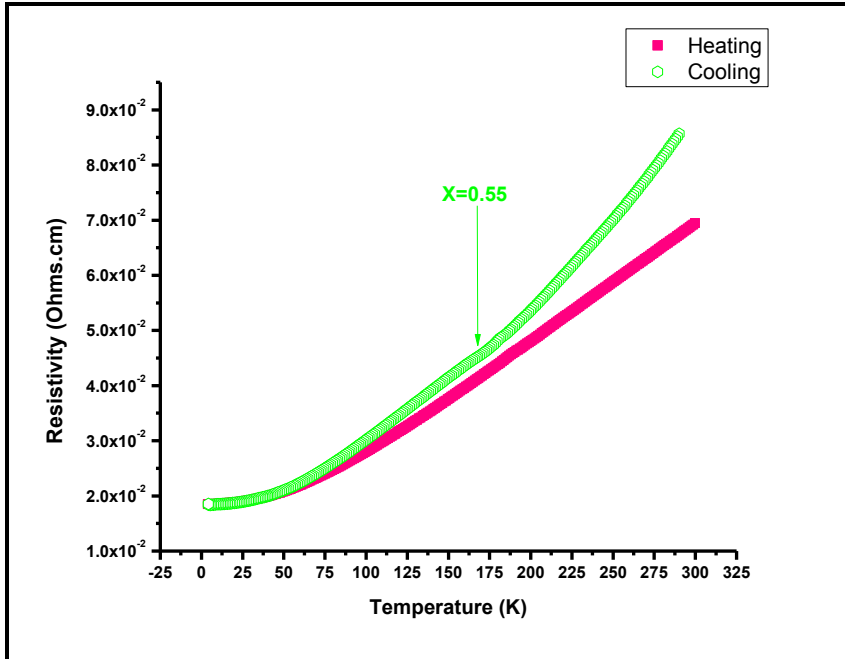


Figure 5.8: Transport measurement for $\text{CrAs}_{0.45}\text{Sb}_{0.55}$ sample

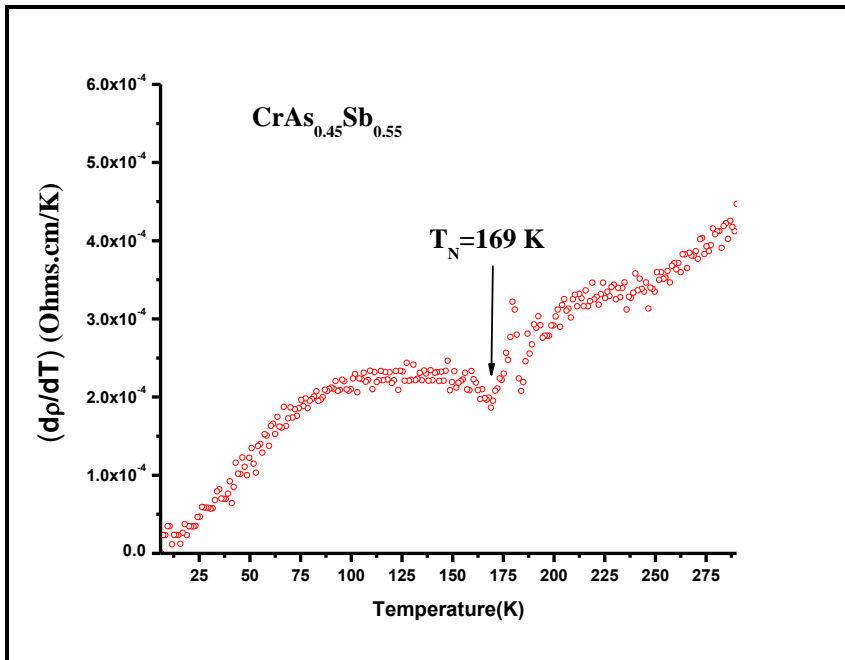


Figure 5.9: Derivative of the resistivity with respect to temperature

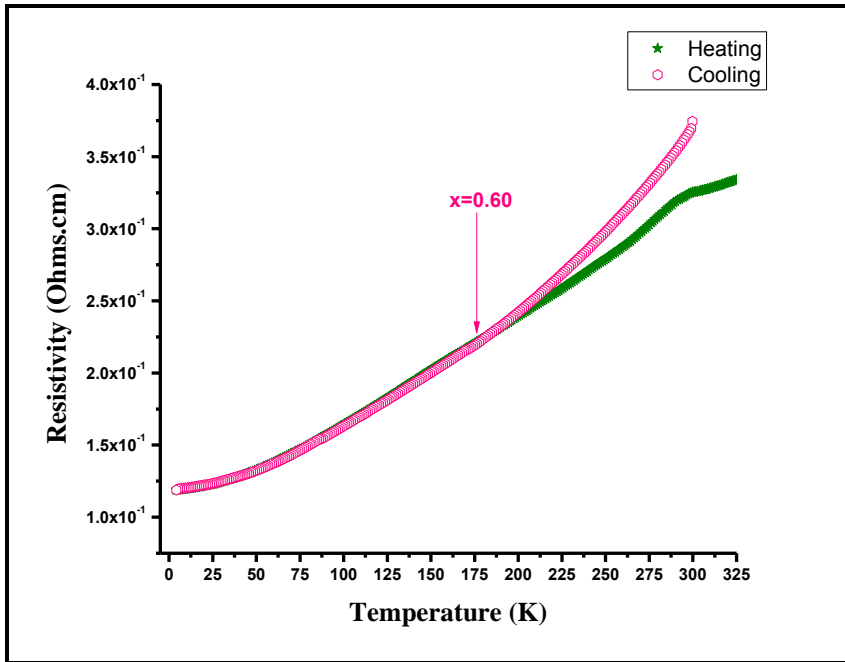


Figure 5.10: Transport measurement for $\text{CrAs}_{0.40}\text{Sb}_{0.60}$ sample

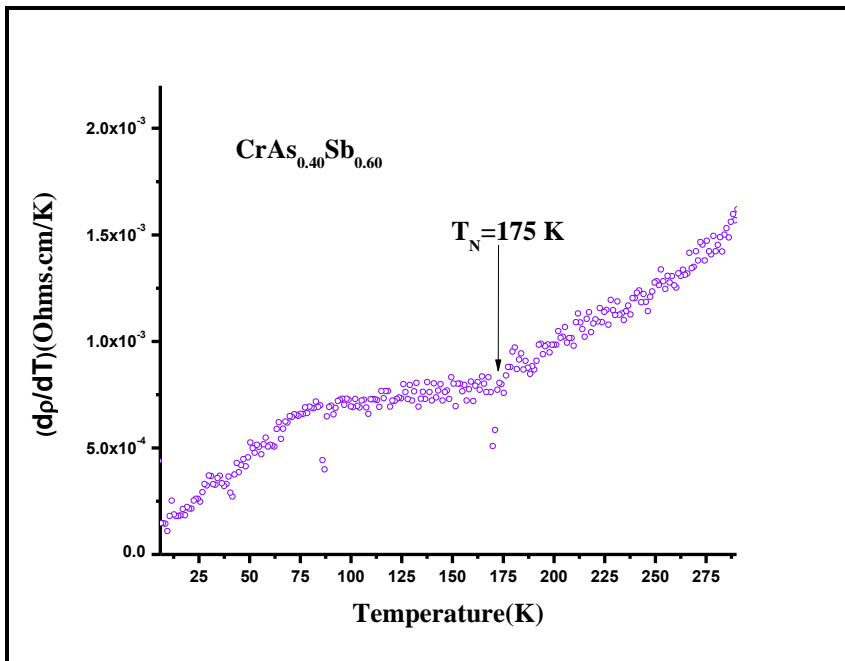


Figure 5.11: Derivative of the resistivity with respect to temperature

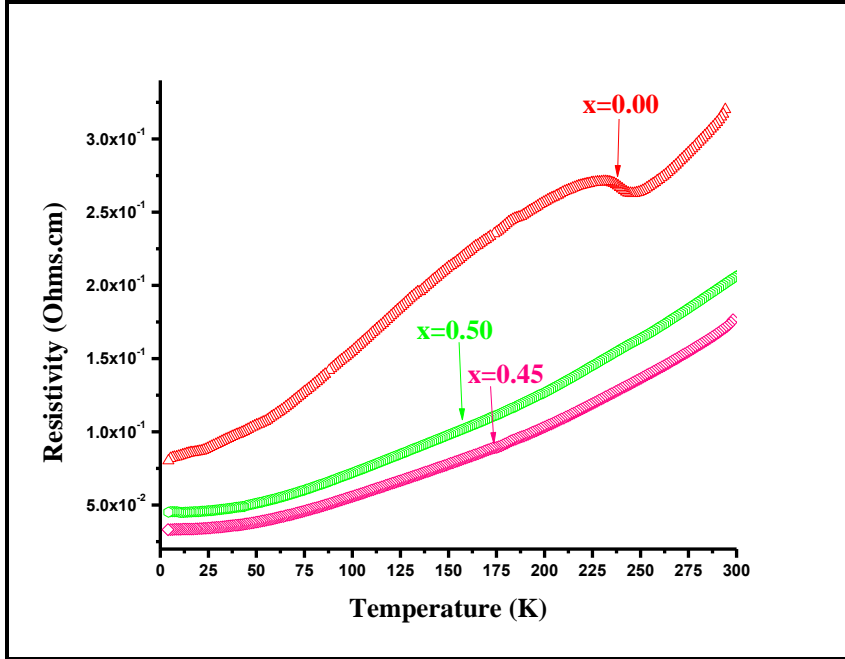


Figure 5.12: Resistivity versus temperature for $\text{CrAs}_{1-x}\text{Sb}_x$ with concentration $x=0.00, 0.45$ and 0.50 .

The variations of the antiferromagnetic transition temperature with Sb concentration is compiled in Table 5.1 and presented in Figure 5.14. The figure shows a sharp linear drop in T_N near $x = 0.45$ with a slop $\sim -10.67 \text{ K}/ x\%$. This is similar to drop in T_N observed in the variations of T_N with applied pressure reported in Figure 5.13 as in [1], the liner slop in this T_N versus pressure phase diagram $\sim -31.43 \text{ K}/\text{kbar}$. The similarity between the antimony substitution and pressure effect in suppressing the antiferromagnetic transition is striking and deserved further investigation in CrAs single crystal. The antiferromagnetic transition temperature and how its value change with concentration of antimony in $\text{CrAs}_{1-x}\text{Sb}_x$ samples as well as the applied pressure on CrAs as in [1] are summarized in Table 5.1 and illustrated in Figure 5.14.

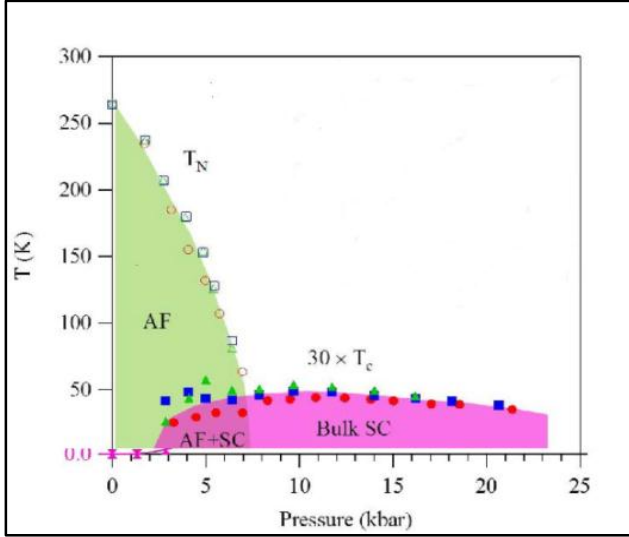


Figure 5.13: phase diagram of CrAs as in [1]

Table 5.1: Antiferromagnetic transition temperature T_N with concentration of Antimony for $(CrAs_{1-x}Sb_x)$ samples and with applied pressure on CrAs as in [1]

Sb x (%)	T_N (K) (this work)	Sb x (%)	T_N Ref.[21]	P (kbar)	T_N (K) Ref.[1]
0	240	0	255	0.00	264
45	175	10	319	2.14	236
50	153	20	351	2.86	207
55	169	30	343	4.28	156
60	175	40	255	5.00	153
		70	438	5.47	129
		80	500	5.71	108
				6.66	86
				6.90	64

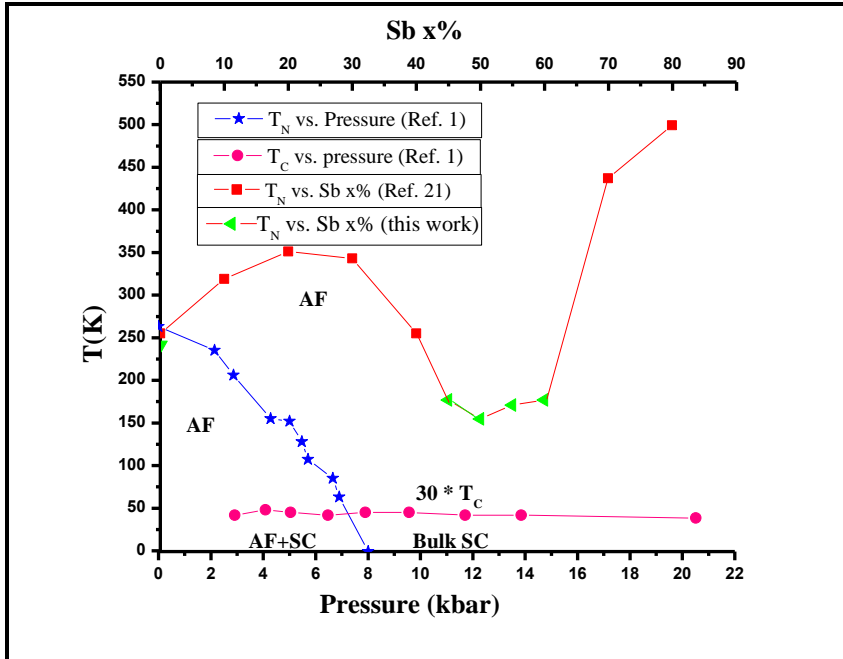


Figure 5.14 Antiferromagnetic transition Temperature in (K) versus Sb x(%) in $\text{CrAs}_{1-x}\text{Sb}_x$ and versus applied pressure on CrAs as in[1]

CHAPTER 6

CONCLUSION AND RECOMENDATION

6.1 Conclusion

This thesis work investigates the effects of antimony substitutions on structural, transport, electronic and magnetic properties of $\text{CrAs}_{1-x}\text{Sb}_x$ system. X-ray diffraction patterns have been used to determine the structure of the samples, lattice parameters and how it is changed upon varying Sb concentration. We found that a significant changes in a, b and c lattice parameters were occurred at $x = 0.45$. The parameters a and b sharply decrease, while c dramatically increases. Moreover, the structure of $\text{CrAs}_{1-x}\text{Sb}_x$ changed from orthorhombic to hexagonal at $x = 0.45$, which has a smaller unit cell volume than orthorhombic as we observed at low concentration of Sb with $x \leq 0.15$. We claim that structure transformation; hence the contraction of volume of unit cell is the main factor for suppressing the antiferromagnetic transition temperature. XPS has been used to determine the chemical composition and the valence state of elements in the surface of the samples. We found that Cr and Sb composition consistent with nominal value. The As atomic ratio is higher than nominal; we attribute this to the segregation of As on the surface of the samples. Moreover, the valence states for the elements are Cr^{+3} , As^{-3} and Sb^{-3} , and it's unchanged upon varying Sb concentration. Transport measurements reveal appoints of inflection in resistivity-temperature graphs. We ascribed these points to the antiferromagnetic phase transition. The antiferromagnetic transition temperature for CrAs was observed at $T_N = 240$ K. A large liner drop in T_N was also observed at $x = 0.45$ with linear slope $\sim -10.67 \frac{\text{K}}{x\%}$. In a way much similar to the drop of T_N for CrAs under the effects of external pressure as recently observed. Subsequently, the magnetic transition

temperatures were used to generate the phase diagram of $\text{CrAs}_{1-x}\text{Sb}_x$ as upon varying the antimony concentration.

6.2 Recommendation for future work

1. One may consider investigating various properties of Single crystals of $\text{CrAs}_{1-x}\text{Sb}_x$ with intermediate concentration of antimony.
2. One may investigate the effects of elemental substitution of phosphorus on the arsenic site of CrAs.
3. The effects of external pressure on the magnetic, transport and structural properties of $\text{CrAs}_{1-x}\text{Sb}_x$ and $\text{CrAs}_{1-x}\text{P}_x$ can also be studied.

References

- [1] W. Wu, J. Cheng, K. Matsubayashi, P. Kong, F. Lin, C. Jin, *et al.*, "Superconductivity in the vicinity of antiferromagnetic order in CrAs," *Nature communications*, vol. 5, 2014.
- [2] N. M. Ashcroft, N. . (1976). *Solid State Physics*.
- [3] C. Kittel. (2010). *Introduction to Solid State Physics*.
- [4] E. Laynton. (1969). *Superconductivity*.
- [5] J. G. Bednorz and K. A. Müller, "Possible highT_c superconductivity in the Ba–La–Cu–O system," *Zeitschrift für Physik B Condensed Matter*, vol. 64, pp. 189-193, 1986.
- [6] Y. Kamihara, T. Watanabe, M. Hirano, and H. Hosono, "Iron-Based Layered Superconductor La [O_{1-x} F_x] FeAs (x= 0.05-0.12) with T_c= 26 K," *Journal of the American Chemical Society*, vol. 130, pp. 3296-3297, 2008.
- [7] H. Takahashi, K. Igawa, K. Arii, Y. Kamihara, M. Hirano, and H. Hosono, "Superconductivity at 43 K in an iron-based layered compound LaO_{1-x}F_xFeAs," *Nature*, vol. 453, pp. 376-378, 2008.
- [8] H. Oh, J. Moon, D. Shin, C.-Y. Moon, and H. J. Choi, "Brief review on iron-based superconductors: are there clues for unconventional superconductivity?," *arXiv preprint arXiv:1201.0237*, 2011.
- [9] M. Rotter, M. Tegel, and D. Johrendt, "Superconductivity at 38 K in the iron arsenide (Ba_{1-x}K_x)Fe₂As₂," *Physical Review Letters*, vol. 101, p. 107006, 2008.

- [10] X. Wang, Q. Liu, Y. Lv, W. Gao, L. Yang, R. Yu, *et al.*, "The superconductivity at 18 K in LiFeAs system," *Solid State Communications*, vol. 148, pp. 538-540, 2008.
- [11] Y. Zhang, Y. Chen, Y. Cui, C. Cheng, H. Zhang, and Y. Zhao, "A study of the Fe-based superconductor $\text{SmFeAsO}_{1-x}\text{F}_x$ by x-ray photoelectron spectroscopy," *Superconductor Science and Technology*, vol. 22, p. 015007, 2009.
- [12] Y. Shen, Q. Wang, Y. Hao, B. Pan, Y. Feng, Q. Huang, *et al.*, "Structural and magnetic phase diagram of CrAs and its relationship with pressure-induced superconductivity," *arXiv preprint arXiv:1409.6615*, 2014.
- [13] A. K. K. Selte, W.E. Jamison, A.F. Andressen, J.E. Engebretsen., "Magnetic Structure and properties of CrAs," *Acta Chemica Scandinavica*, vol. 25, pp. 1703-1714, 1971.
- [14] H. W. N. Kazama, *J. Phys. Soc. Japan*, vol. 30, p. 1319, 1971.
- [15] H. Boller and A. Kallel, "First order crystallographic and magnetic phase transition in CrAs," *Solid State Communications*, vol. 9, pp. 1699-1706, 1971.
- [16] A. K. H. Boller, *Solid State Commun*, vol. 9, p. 1666, 1971.
- [17] T. Suzuki and H. Ido, "Spontaneous magnetostriction of $\text{CrAs}_{1-x}\text{S}_x$ compounds," *Journal of magnetism and magnetic materials*, vol. 140, pp. 149-150, 1995.
- [18] A. J. Kjekshus, Warren E., "The Magnetic Properties of $\text{CrAs}_{(1-x)}\text{Se}_x$." *Acta Chemica Scandinavica*, vol. 25, pp. 1715-1721, 1971.
- [19] H. I. T. Suzuki, *J. Appl. Phys.*, vol. 73, p. 5688, 1993.

- [20] K. Kanaya, S. Abe, H. Yoshida, K. Kamigaki, and T. Kaneko, "Magnetic and structural properties of pseudo-binary compounds $\text{CrAs}_{1-x}\text{Px}$," *Journal of alloys and compounds*, vol. 383, pp. 189-194, 2004.
- [21] T. Suzuki and H. Ido, "Crystallographic and magnetic properties of $\text{CrAs}_{1-x}\text{Sbx}$," *Journal of Magnetism and Magnetic Materials*, vol. 54, pp. 935-936, 1986.
- [22] H. Watanabe, N. Kazama, Y. Yamaguchi, and M. Ohashi, "Magnetic Structure of CrAs and Mn-Substituted CrAs ," *Journal of Applied Physics*, vol. 40, pp. 1128-1129, 1969.
- [23] T. Suzuki and H. Ido, "Magnetic and crystallographic properties of $\text{Cr}_{1-x}\text{Ti}_x\text{As}$ ($0 \leq x \leq 1$)," *Journal of Applied Physics*, vol. 55, pp. 2042-2044, 1984.
- [24] L. Keller, J. White, M. Frontzek, P. Babkevich, M. Susner, Z. Sims, *et al.*, "Pressure dependence of the magnetic order in CrAs : a neutron diffraction investigation," *arXiv preprint arXiv:1409.5706*, 2014.
- [25] J. Jeffries, N. Butch, H. Cynn, S. Saha, K. Kirshenbaum, S. Weir, *et al.*, "Interplay between magnetism, structure, and strong electron-phonon coupling in binary FeAs under pressure," *Physical Review B*, vol. 83, p. 134520, 2011.
- [26] J.-K. Bao, J.-Y. Liu, C.-W. Ma, Z.-H. Meng, Z.-T. Tang, Y.-L. Sun, *et al.*, "Superconductivity in quasi-one-dimensional $\text{K}_2\text{Cr}_3\text{As}_3$," *arXiv preprint arXiv:1412.0067*, 2014.
- [27] Z.-T. Tang, J.-K. Bao, Y. Liu, Y.-L. Sun, A. Ablimit, H.-F. Zhai, *et al.*, "Unconventional superconductivity in quasi-one-dimensional $\text{Rb}_2\text{Cr}_3\text{As}_3$," *arXiv preprint arXiv:1412.2596*, 2014.

- [28] J.-K. Bao, J.-Y. Liu, C.-W. Ma, Z.-H. Meng, Z.-T. Tang, Y.-L. Sun, *et al.*, "Superconductivity in Quasi-One-Dimensional $K_2Cr_3As_3$ with Significant Electron Correlations," *Physical Review X*, vol. 5, p. 011013, 2015.
- [29] J. w. John F. Watts, *An Introduction to SURFACE ANALYSIS by XPS and AES*. UK, 2003.
- [30] S. W. G. N. Winograd, "X-ray Photoelectron Spectroscopy," vol. 2, pp. 16-152, 1980.
- [31] H. H. K. Selte, A. Kjekshus, A.F. Andressen, *Acta Chem. Scand*, vol. A29, p. 312, 1975.
- [32] A. Kallel, M. Nasr-Eddine, and H. Boller, "Crystallographic distortion in $CrAs_{0.50}Sb_{0.50}$," *Solid State Communications*, vol. 12, pp. 665-671, 1973.
- [33] N. Stojilovic, "Why Can't We See Hydrogen in X-ray Photoelectron Spectroscopy?," *Journal of Chemical Education*, vol. 89, pp. 1331-1332, 2012.
- [34] L. R. M. Moffat T.P., Ruf R.R., *Electrochim. Acta*, vol. 40, p. 1723, 1995.
- [35] I. H. Mizokawa Y., Nishitani R., Nakamura S., *J. Electron Spectrosc. Relat. Phenom.*, vol. 14, p. 129, 1978.
- [36] Y. W. T. Liu W.K., Stradling R.A., *J. Vac. Sci. Technol.*, vol. B 13, p. 1539, 1995.
- [37] G. F. J. Vasquez R.P., *J. Appl. Phys.*, vol. 52, p. 3509, 1981.
- [38] F. D. Wang J., Wu W., Zeng M., Li Y., *Polymer Degradation and Stability*, vol. 31, p. 129, 1991.
- [39] P. Godowski, D. Costa, and P. Marcus, "Surface segregation of arsenic in iron," *Journal of materials science*, vol. 30, pp. 5166-5172, 1995.

- [40] H. Kotegawa, S. Nakahara, H. Tou, and H. Sugawara, "Superconductivity of 2.2 K under pressure in helimagnet CrAs," *Journal of the Physical Society of Japan*, vol. 83, p. 093702, 2014.

Vitae

Name : Mohammed Abdallah Khalid Abubaker

Nationality : Palestinian

Date of Birth : 11/6/1990

Email : mham125ad@gmail.com

Telephone : +966537060339, +970598013577

Address : Yabed-Jenin-Palestine

Academic Background :

1. M.S. in Condensed matter Physics. King Fahd University of Petroleum and Minerals, Dhahran - Saudi Arabia (2015).
2. B.S. in Physics. Al-Najah National University, Nablus- Palestine (2012).
3. The General Secondary Certificate in Scientific Stream. Yabed secondary School, Jenin - Palestine (2008).